Control Augmentation for Lateral Control Wheel Steering

Final Report

NASA Grant NAG 1-88

Youngstown State University
Youngstown, Ohio 44555

Principal Investigator:

Dr. Robert H. Foulkes, Jr.

Technical Monitor:

Dr. Jeremiah F. Creedon
Flight Electronics Division
NASA Langley Research Center
Hampton, Virginia 23665

August 13, 1981

Control Augmentation for Lateral Control Wheel Steering

Abstract

This report, the final report for NASA Grant NAG 1-88, discusses flight control system design for lateral control wheel steering. Following initial work by the Boeing Company and the Flight Electronics Division of Langley Research Center, two alternate designs are presented. The first design is a roll-rate command, bank-angle hold system with a wings-level track-hold submode. The second is a curved-track-hold system. Design details and real-time flight simulator results are included.

Table of Contents

List of Figures

List of Symbols and Symbolic Names

Symbol	Units	Description
ACSL	N/A	Advanced Continuous Simulation Language
AILCMD	degrees	Lateral CWS control system output to aileron servo
CAS	knots	Calibrated airspeed
CWS	N/A	Control Wheel Steering
DPED	inches	Pilot's pedal input
DWHL	degrees	Pilot's wheel input
EADI	N/A	Electronic Attitude Director Indicator
EHSI	N/A	Electronic Horizontal Situation Indication
GTNPHC	ft/sec^2	Configuration D crosstrack acceleration command
PHCMD1, ϕ_{c1}	degrees	Wheel-derived bank angle command
PHCMD3	deg/sec	Wheel-derived component of roll-rate command
PHCMD4, ϕ_{c4}	degrees	XTK-loop output
PHI, ϕ	degrees	Bank angle
PHICMD, ϕ_c	degrees	Total bank angle command
PHIDOT	deg/sec	Rate of change of bank angle (roll rate)
PHIDTC	deg/sec	Roll-rate command
PSI	degrees	Airplane heading angle
RTS	N/A	Real-time flight simulator
RUDCMD	degrees	Lateral CWS control system output to rudder servo

Symbol	Units	Description
TK, PSIG	degrees	Ground track angle
VGS	ft/sec	Ground speed
XTK	ft/sec^2	Crosstrack acceleration
XTKC	ft/sec^2	Crosstrack acceleration command
XTKX	ft/sec	Relative track angle command signal
YE	feet	Crosstrack position error
q	deg/sec	Pitch rate
γ	degrees	Flight path angle
γ_c	degrees	Flight path angle command
$\dot{\gamma}$	deg/sec	Rate of change of flight path angle
ϕ_e	degrees	Error between total bank angle command and bank angle

1. INTRODUCTION AND BACKGROUND

1.1 Introduction

The level of activity at commercial airports has increased drastically during the past two decades. Attendent with this increase are increases in the number and intensity of problems associated with airport traffic, problems such as air traffic congestion, high noise levels near airports, and delays and diversions caused by weather effects. In an attempt to alleviate some of these problems, NASA and the FAA have jointly initiated the Terminal Configured Vehicle (TCV) program, a long term research effort conducted by NASA Langley Research Center and aimed at the development of improved airborne system capability and advanced ground-based facilities [1].[1]

Among the objectives of the TCV program is the capability for precise control along steep, curved flight paths. Such paths would result in more efficient scheduling of arriving aircraft, avoidance of sensitive areas, and reduced noise intensity for areas near airports.

Precise control along steep, curved paths, however, leads to more stringent requirements for aircraft control, which in turn, lead to an increased number of complex

---

[1]Numbers in square brackets denote references at the end of the report.

tasks for the pilot during manual aircraft maneuvering. Pilot workload can be reduced by improved airborne control systems that give the pilot direct control over the flight path while providing automatic control to handle transient responses to aircraft trim changes or disturbance (wind) inputs.

The work discussed in this report deals with the design of a control system for the lateral axes. Section 1.2 contains background on a longitudinal control system design and previous lateral control systems designs. Sections 2 and 3 contain two alternate lateral control system designs. In section 2, a roll-attitude-hold design with wings-level ground-track-hold capability is presented, while section 3 contains the design of a curved-track-hold system. Some conclusions and recommendations are presented in section 4.

1.2 Background

As part of the TCV program, NASA Langley Research Center and the Boeing Company have collaborated on the development of a system to provide the pilot with direct command of the flight path and with a visual display of flight path parameters such as flight path angle, ground track, and aircraft attitude. Direct command of the flight path is accomplished by enabling the pilot to control

the magnitude and direction of the velocity vector. Hence, the system has been called the Velocity Vector Control Wheel Steering and Display System, or velocity CWS system [2].

The overall velocity CWS system contains three subsystems: (1) a longitudinal velocity CWS system to provide flight path angle control, (2) a lateral velocity CWS system to provide turn radius or track angle control, and (3) an autothrottle system for control of the magnitude of the velocity vector.

An overall velocity CWS system for the NASA TCV B-737 aircraft is discussed in [2]. Specific design configurations are presented for a longitudinal velocity CWS system and two alternate lateral velocity CWS systems. A detailed development of the longitudinal design is presented in [3]; the resulting design is shown in Figure 1. The design includes (1) rate feedback (q and $\dot{\gamma}$) for inner loop stability and damping, (2) a commanded flight path angle (γ_c) derived from the pilot's column input, and (3) position feedback with proportional-plus-integral compensation to control the actual flight path angle (γ) to the commanded angle (γ_c). One further aspect is worth noting. The transfer function zero produced by the proportional-plus-integral compensation causes overshoot in the γ-response. The overshoot was minimized by preventing the integrator output from becoming too large during the transient response by adding a $\dot{\gamma}$ term to the integrator input that opposes the position error term.

The Boeing work on a lateral velocity CWS system resulted in two alternate designs, configuration A, shown in Figure 2, and configuration B, shown in Figure 3 [2,4]. Configuration A is a roll-attitude-hold design with a track-hold submode for a wings-level condition, while B is a curved-track-hold design. Both configurations used roll rate feedback for inner loop stability and damping, and bank angle feedback with proportional compensation for position control. Both configurations also have a pedal-only decrab maneuver in which a signal is crossfed from pedal to bank angle command to produce the bank angle needed to maintain ground track during the decrab maneuver. In addition, A and B both use a turn coordinator in which the bank angle is processed through a washout filter to produce a rudder command whenever the bank angle changes. The rudder command produces a yawing moment that reduces sideslip during the transient portion of a turn.

In configuration A, the wheel input is integrated to give the bank angle command; the control system brings the bank angle to the commanded value and maintains it there. If a wings-level condition is commanded, an additional loop in which normal or crosstrack acceleration is fed back is closed. While the loop is closed, the crosstrack acceleration is used to maintain the ground track angle established when th loop was closed.

In configuration B, the integral of the wheel input gives a commanded curvature, which, when multiplied by the square of the ground speed, produces an acceleration command. A bank angle command is processed from the acceleration command, and the bank angle maintained at this value by the position control loop. In addition, a crosstrack acceleration loop essentially identical to the one in configuration A operates continously to maintain the acceleration at the commanded value. The net result is that the pilot can command a radius of curvature, and the control system computes the bank angle necessary to fly that radius and keeps the actual bank angle at the computed value.

The control systems described above form an inner loop for automatic control of perturbations in the flight path. The commanded flight path is selected by the pilot in an outer control loop. Feedback in this loop is provided by a visual display of flight path parameters. The display has two components: a vertical situation display, or Electronic Attitude Director Indicator (EADI), and a horizontal situation display, or Electronic Horizontal Situation Indication (EHSI) [2]. The EADI, shown in Figure 4, displays flight path angle and airplane attitude. The EHSI, shown in Figure 5, displays the ground track.

In order to evaluate velocity CWS control system performance, two computer simulations of the control law along with the NASA TCV B-737 dynamics are available.

The first is a batch simulation using the Advanced Continuous Simulation Language (ACSL); the second is the NASA real-time piloted flight simulator (RTS).

RTS results for configurations A and B are shown in Figures 6 and 7. Configuration A responses for a variety of flight conditions are given in Figure 6, and configuration B responses in Figure 7. In each case, a bank angle of approximately 20 degrees was commanded, followed by a wings-level command about 20 seconds later. The configuration A bank angle command (ϕ_c) contains a transient oscillation when the wings-level condition is commanded. This oscillation occurs when the track-hold submode is engaged by closing the crosstrack acceleration loop. Because that loop is closed continuously in configuration B, the ϕ_c response in Figure 7 shows similar oscillations for both the wings-level command and the 20 degree bank angle command.

The orginal aileron and spoiler servo models used in the RTS program did not contain modifications to the servos that correct stability problems that existed in the roll axis on the TCV B-737 aircraft. The changes included addition of a lead-lag filter in the aileron servo to increase stability margin and addition of spoiler feedback to de-emphasize the nonlinear effect of the spoilers on the rolling moment coefficient [5].

Updated models for the aileron and spoiler servos were developed by Information & Control Systems, Inc., and

reported in [6]. These models were incorporated into the RTS lateral CWS program. Figure 8 contains a comparison of the servo models using the configuration B roll response. Figure 8(a) shows the response using the original models, and Figure 8(b) using the updated models. The nonlinear element causing the limit cycle in Figure 8(a) was determined to be the aileron hysteresis model in the original aileron servo model.

With the exception of Figure 8(a), all RTS results shown in this report use the updated models.

2. LATERAL VELOCITY CWS: CONFIGURATION C

In this section, a third lateral velocity CWS control system, called configuration C, is discussed. It is essentially a modification of the configuration A control law discussed above. The configuration C control law is shown in Figures 9 - 12. The roll attitude control loop, track-angle control loop, and pedal-only decrab loop are discussed in the sections below.

2.1 Roll Attitude Control

In view on the fact that both configurations A and B (Figures 2 and 3) use the same control loop for roll attitude, it was decided to begin the control law modification with this loop. A review of the longitudinal design [3] showed that increased inner loop damping from rate feedback along with proportional-plus-integral compensation for position control provided satisfactory performance in the flight path angle response. A similar approach was tried for the lateral control system.

Configuration C is a roll-rate-command, roll-position-hold control system. The wheel input is used to calculate a commanded bank angle PHCMD1 (see Figure 9), which is displayed on the EADI. The control system brings the actual bank angle PHI, also displayed on the EADI, to the commanded value and maintains it there.

Inner loop damping is provided by roll rate feedback and the gain KPHIDT as in configuration A. The gain KPHIDT in configuration C is analogous to the product of KPHIDT and the two gain schedules F_2(CAS) and KV(CAS) (see Figure 2 and [2]). For convenience, this product is sketched in Figure 13. Simulation results indicated that a substantially higher KPHIDT would improve damping without adversely affecting stability.

Position control is provided by bank angle feedback and proportional-plus-integral compensation (gains K1 and K2). A roll-rate term (gain K3) is subtracted from the integrator input to prevent the output from becoming too large during the transient portion of a turn.

In addition to the output of the proportional-plus-integral compensation, the roll-rate command PHIDTC contains a signal PHCMD3 which results from passing PHCMD1 through a wash-out filter. Thus PHIDTC contains a signal essentially proportional to the wheel input. This signal tends to reduce the initial lag in the bank angle response to a wheel input.

Initially the design of configuration C included the same turn coordinator used in configuration A (see Figure 2). RTS results showed, however, that if the pilot changed the flap setting from below 20° to above 20° during a turn, the turn coordinator produced an unwanted transient. A second problem involved the effect of opening

or closing the feedback loop containing the turn coordinator on the basic roll attitude control dynamics. The FLAPS $\leq$ 20 response differed enough from the FLAPS > 20 response that a change in gains (K0, K1, K2, and K3) was necessary to produce sufficiently similar responses.

To remedy these problems, a new turn coordinator using the PHCMD3 signal was designed. Simulation results indicated that PHCMD3 is similar to PHIDOT and that suitable choices for KTC and TAUTC yield similar results to the original turn coordinator, but without the first problem mentioned above. The second problem could be solved by programming the flap-controlled switch so that the turn coordinator was gradually removed as the flight condition (i.e., flap setting) changed. The turn coordinator and gain schedule for FPSW are shown as part of configuration C in Figure 9.

Figure 14 shows the configuration C attitude-hold response for a variety of flight conditions. In each case, the wheel input was 15 degrees for 3 seconds, resulting in a commanded bank angle of approximately 20 degrees. Also, in each case, the gains, time constants, and limits were set at the nominal values given in Figure 9.

During piloted RTS sessions, it was noted that, under certain flight conditions, the pilot could command PHCMD1 to increase at a rate faster than the airplane could follow. Limiting of the actual roll rate was apparently

due to aileron position limiting as well as decreases in the aileron effectiveness and spoiler effectiveness at certain speed and flap combinations. The worst case condition seemed to be around 210 knots with no flaps and gear up. At this flight condition, limiting of the roll rate caused an unstable response when the pilot commanded a 50 to 60 degree change in bank angle at full wheel input.

The problem was corrected by limiting the input to the PHCMD1-integrator. A limit of 10 degrees/second eliminated the unstable response without adversely affecting more normal roll rate commands. Subsequent RTS testing indicated satisfactory performance over the entire flight regime.

2.2 Track-Angle-Hold Submode

Figure 9 shows a feedback loop in which crosstrack acceleration (XTK) is processed to produce a signal PHCMD4. PHCMD4 is combined with PHCMD1 to yield the total bank angle command PHICMD. As long as the pilot commands a condition other than wings-level ($|PHCMD1| > 2.5°$), the YDTERR and YERR integrators are reset to zero and PHCMD4 is zero. This produces the normal roll-attitude-hold performance.

When a wings-level condition is commanded and the bank angle becomes sufficiently small, the logical variable IC1 becomes false and the YDTERR and YERR integrators

begin to operate, in effect closing the XTK-loop. The loop is designed to produce a bank angle command that keeps the ground track angle at the value it was when the loop was closed. In order to reduce the transient that results from closing the XTK-loop, the crosstrack acceleration is commanded to zero smoothly using the XTKC signal.

If the pilot returns the wheel to detent with $|PHCMD1| < 2.5°$ but $PHCMD1 \neq 0$, it is commanded to zero smoothly by closing the feedback loop around the PHCMD1-integrator. A logical variable SWT1 controls this loop. The logic controlling IC1 and SWT1 is found in Figure 10.

Figure 9 also shows a signal XTKX being fed into the XTK-loop. The logic and calculations used to determine XTKX are shown in Figures 11 and 12. A lateral thumb switch on the brolly handle allows the pilot to command a 0.5 degree change in track angle in either direction. The XTKX signal in Figure 9 causes the necessary bank angle change to produce the desired track angle change. The logic in Figure 11 prevents a relative track angle command input unless the XTK-loop is closed. The signal TKC is the actual track angle at the time the XTK-loop is closed plus the relative track angle command and is displayed as a commanded track angle on the EADI.

RTS results have showed satisfactory behavior for both the transient response caused by closing the XTK-loop and the track-angle-hold capability in the presense of

gusts. Figure 15 shows the transient response to a wings-level command for a variety of flight conditions.

2.3 Pedal-Only Decrab Maneuver

The pedal-only decrab maneuver in configuration C is essentially the same as it is in A and B. While the pilot selects a pedal input to decrab the airplane, a signal is crossfed from pedal to bank angle command. This signal along with the XTK-loop produces the bank angle needed to keep the airplane on track as long as the pedal input is being applied.

The differences in the pedal crossfeed between configuration C and configurations A and B are as follows. First, the decrab maneuver can be performed only for flap settings of 30° and 40° in C, while it could also be performed at flaps 25° in A and B. Second, to prevent the engine nacelle from hitting the ground, the crossfeed limit was reduced from 9° to 5°. Finally, the gain KDELR was reduced.

It was noticed during piloted RTS sessions that there was a substantial transient oscillation during the decrab maneuver. ACSL simulation showed a similar behavior as indicated in Figure 16. The relatively large transient oscillation in the bank angle (Figure 16(a)) caused the variation in track angle seen in Figure 16(b). Although the steady-state track angle was the same as the initial

value, the transient caused a relatively large track error (YE) (Figure 16(c)). Figure 17 shows the same responses with PEDLIM reduced from 9° to 5° and KDELR reduced from 6.0 to 2.5. Subsequent RTS testing with these values indicated satisfactory performance.

3. LATERAL VELOCITY CWS: CONFIGURATION D

In this section, a lateral velocity CWS control law referred to as configuration D is discussed. Configuration D, essentially a modification of configuration B, is a curved-track-hold system in which the pilot selects a circular ground track using the curved trend vector on the EHSI (Figure 5), and the control system maintains the bank angle necessary to fly that ground track. A block diagram of configuration D is shown in Figure 19.

The actual design of configuration D is a combination of configurations B and C. The discussions in Section 2 of roll attitude control, relative track angle command, and pedal-only decrab maneuver for configuration C also pertain to configuration D. The computations of acceleration and bank angle commands from the wheel input follow directly from B. The XTK-loop in D differs from that in B with respect to the crosstrack acceleration reference signal and the operation of the XTK-loop integrators.

The crosstrack acceleration reference signal $\ddot{y}_c$ in B (see Figure 3) is calculated by passing the commanded acceleration g TAN(ϕ_c) through a 0.75 second first-order lag filter. A slightly different calculation is used in D. The acceleration reference XTKC is lagged from the signal GTNPHC during the transient caused by a wheel input. The amount of lag is determined by the time constant TAUX,

which is calculated to minimize the difference between XTKC and XTK. The calculation is shown in Figure 18, note F. Under steady-state conditions with the wheel in detent, the acceleration reference XTKC equals GTNPHC. Thus, while turning in a steady wind, the crosstrack acceleration command is GTNPHC.

In configuration B, the XTK-loop integrators operate continuously. In D, they are reset to zero at the beginning of the track-hold mode. This mode is considered to begin when the pilot returns the control wheel to detent after having selected a turn radius. In order for the track-hold mode to operate properly in a wings-level condition, the XTKC signal must be zero during the time the integrators operate. Due to the lag in the crosstrack acceleration response, a relatively large transient results if the integrators begin to operate exactly when the wheel is put into detent. To reduce this transient somewhat, the operation of the integrators is delayed until the commanded acceleration is sufficiently small. The logical variable IC2, calculated in note J of Figure 18, controls the XTK-loop.

Figure 19 shows the configuration D roll response to a wheel input for a variety of flight conditions. The responses are similar to the configuration C responses with the exception of the PHCMD4 signal, the output of the XTK-loop. Without the XTK-loop, the bank angle would

follow PHCMD1, which is calculated from the desired turn radius and the actual ground speed, assuming a coordinated turn. Hence, to fly the desired ground track, the crosstrack acceleration should be GTNPHC. The XTK-loop is used to account for any difference between the crosstrack acceleration XTK and GTNPHC. The steady-state value of PHCMD4 is an indication of the magnitude of this difference for the various flight conditions in Figure 19.

The configuration D wings-level track-hold response is shown in Figure 20. The wings-level XTK-loop logic is adjusted so that the integrators remain at zero until the crosstrack acceleration command XTKC decreases to 1 ft/sec^2 or less. The results again are similar to the configuration C responses (see Figure 15).

As shown in Figure 10, the parameter PHILIM controls the point at which the XTK-loop latches on to the desired wings-level ground track. With PHILIM sufficiently large, the wings-level track-hold mode is engaged exactly when SWT1 becomes false, resulting in a relatively large transient in PHCMD4. With PHILIM sufficiently small, the transient is reduced. Figure 21 shows a comparison of results with PHILIM = 100, to those with PHILIM = 1. The flight condition was 120 knots, 5000 feet, flaps 40, and gear down. The difference in steady-state track angle between the two cases was approximately 0.75 degree.

The curved-track-hold performance of configuration D is shown in Figure 22. The airspeed was 210 knots, and, as indicated, the wind speed was 15 knots. Although not evident by inspection, Figure 22 shows three revolutions of the ground track, indicating satisfactory track-hold performance. The only manual input was the wheel input needed to initiate the turn.

For comparison, the performance of configuration C under the same conditions is shown in Figure 23.

4. CONCLUSIONS AND RECOMMENDATIONS

Both configurations C and D have undergone extensive non-piloted RTS testing. The results shown in Figures 14, 15, 19, 20, 21, 22, and 23 come from these tests. Based on these results, the overall performance of both control systems is satisfactory.

In addition, configuration C has undergone piloted evaluation on the flight simulator. Pilot acceptance of the basic roll control dynamics was good, but problems, such as those with the turn coordinator and decrab maneuver (see Sections 2.1 and 2.3), were encountered. With pilot assistance and further RTS testing, these problems were solved.

Following the RTS evaluation, it was decided that configuration C was ready for flight tests. Experimental requirements for software, display, and brolly handle thumb switch were prepared and submitted.

At the writing of this report, pilot evaluation of configuration D has begun. Initial results are consistent with the non-piloted results. Improvements in the turn coordinator, decrab maneuver, and wings-level track-hold mode that were carried through from configuration C perform as well in D.

Configuration D has two problems not found in configuration C. Both problems involved the operation of the

XTK-loop in a non-wings-level condition. The first involved the bank angle command display and the second involved coupling between the longitudinal and lateral control systems.

Because the XTK-loop operates in D in a non-wings-level condition and because PHCMD4 builds to a non-zero steady-state value in a turn, there is a steady-state difference between PHICMD and PHCMD1, hence, between PHI and PHCMD1. Thus the bank angle would exhibit a standoff from the command if PHCMD1 were used to drive the display. Figure 18 shows the $\emptyset_c$-DISPLAY being switched by SWT1 between PHCMD1 and PHICMD. In essence, the switch puts PHCMD4 into the display calculation in a non-wings-level condition.

It was discovered during RTS testing of configuration D that a sustained oscillation existed when a large bank angle (e.g., 40 degrees) was commanded. Further tests indicated that the oscillation appeared in both bank angle and flight path angle and that configuration C had no similar problem. When the XTK-loop was disconnected in configuration D, the oscillation disappeared. Thus, the problem was attributed to the coupling between the longitudinal and lateral airplane dynamics at steep bank angles along with the curved-track-hold capability in configuration D.

Because the oscillation was not apparent at less steep bank angles, it was decided to solve the problem by disconnecting the XTK-loop when the bank angle command PHCMD1 exceeded 30 degrees. The modified XTK-loop is shown in Figure 24.

Without the XTK-loop, the curved-track-hold performance of configuration D will deteriorate. The amount of deterioration in the ground track is indicated in Figure 25. The shift of the ground track approximately perpendicular to the wind direction is due to the small steady-state lag between the crosstrack acceleration XTK and the acceleration command GTNPHC that exists when the XTK-loop is disconnected.

This report concludes with a recommendation that piloted RTS evaluation of configuration D be completed and that preparations be made for flight tests of both configurations. Also, additional efforts, such as the evaluation of the roll axis damping for flight conditions such as 210 knots with no flaps, may improve the performance of both configurations. Simulator results indicate a decrease in damping at flight conditions in the 200 to 250 knot range with little or no flaps as compared to other speed and flap combinations. A related effect involves the reduced use of the turn coordinator for low flap settings. The PHCMD4 signal in the configuration D roll response (Figure 19) indicates that increased use of the turn

coordinator at lower flap settings may improve the transient response.

Coupling between the longitudinal and lateral CWS control systems provides another area for further work. Research efforts spent on decoupling approaches as well as integrated designs may well enhance the performance of overall CWS systems.

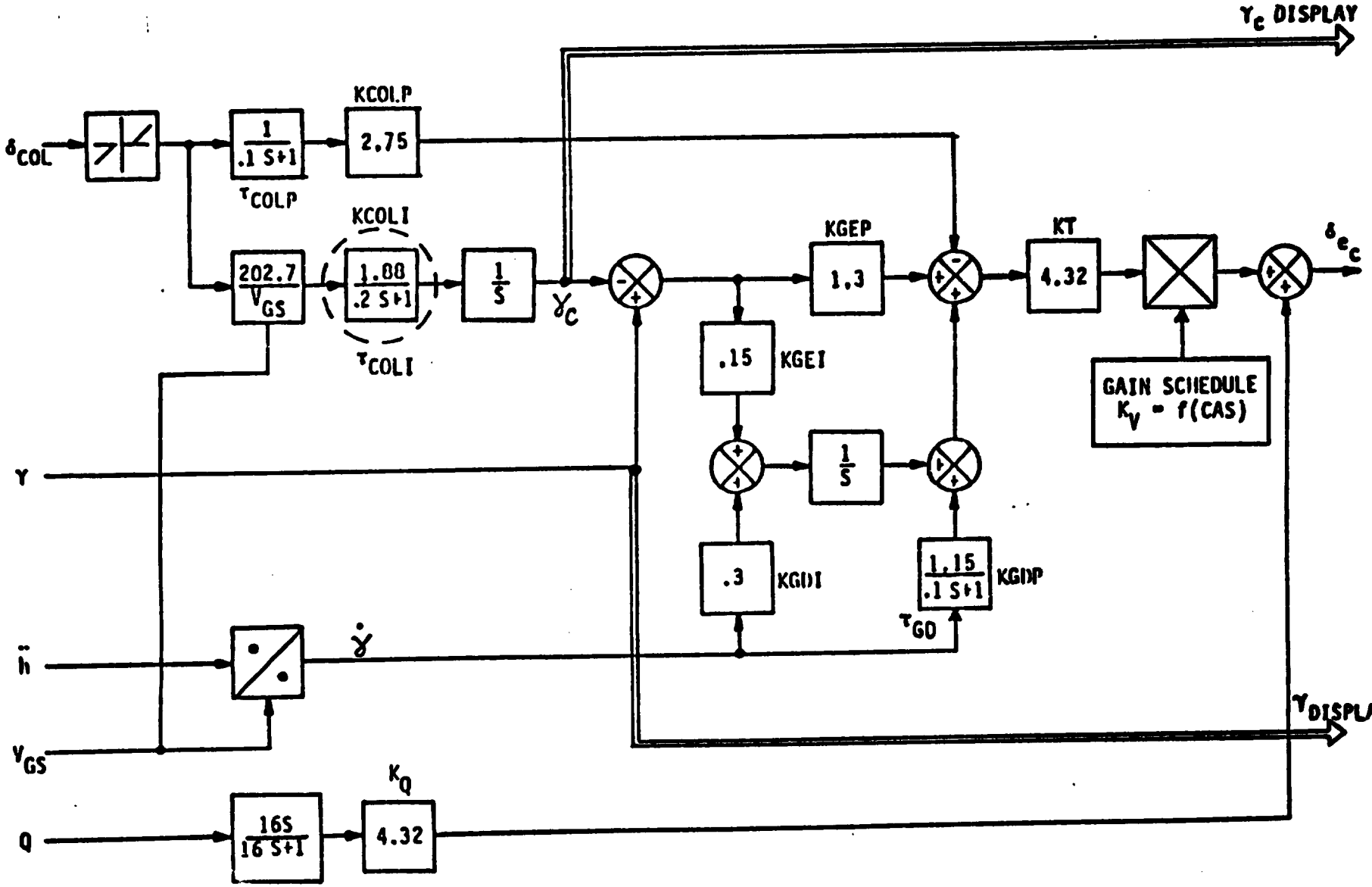

Figure 1. - Longitudinal velocity CWS system (from [3]).

RATE COMMAND ATTITUDE HOLD/TRACK HOLD VELOCITY CONTROL WHEEL STEERING CONTROL LAW

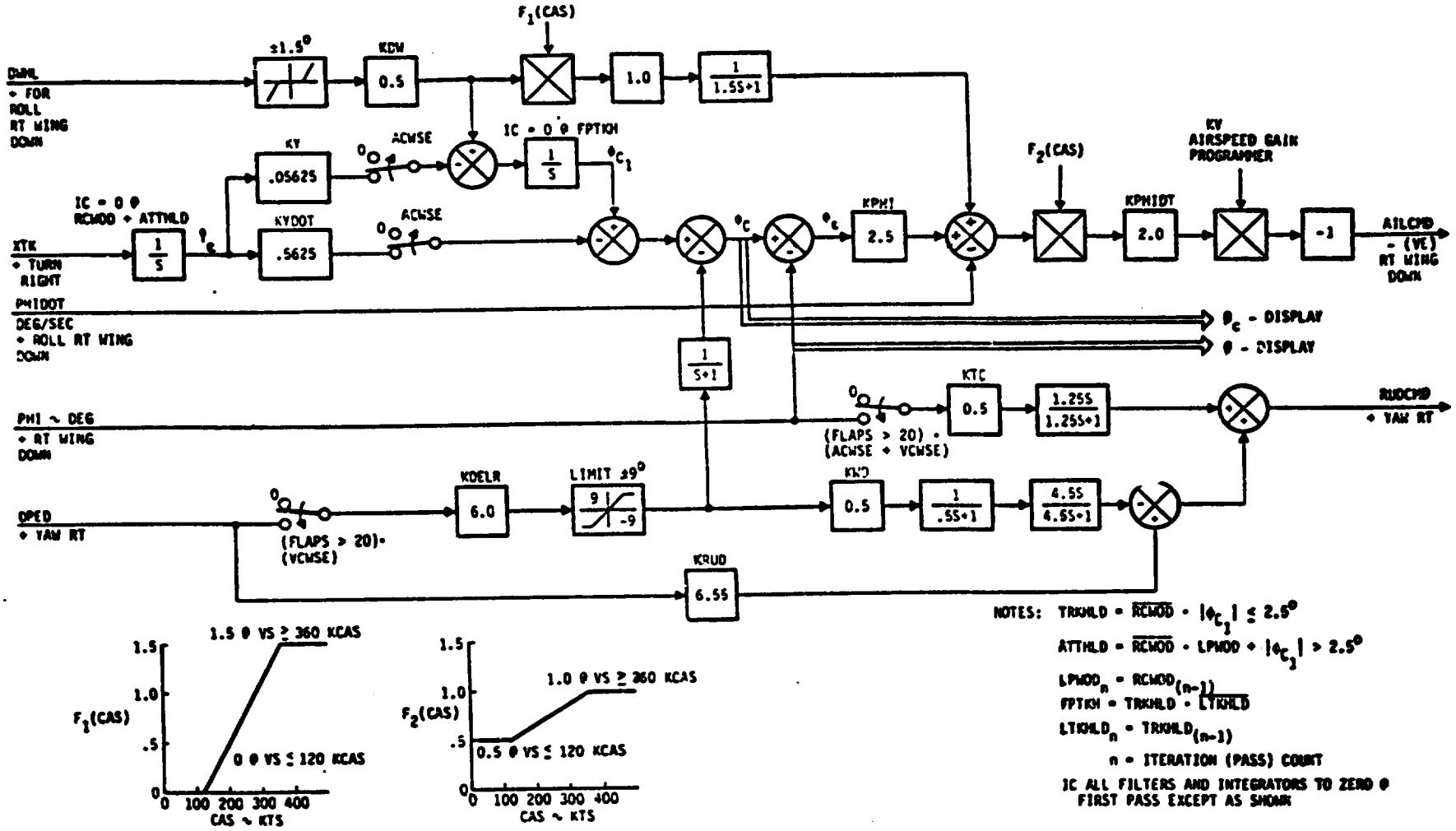

Figure 2. - Configuration A lateral velocity CWS system (from [4]).

CURVED TRACK COMMAND VELOCITY CONTROL WHEEL STEERING CONTROL LAW

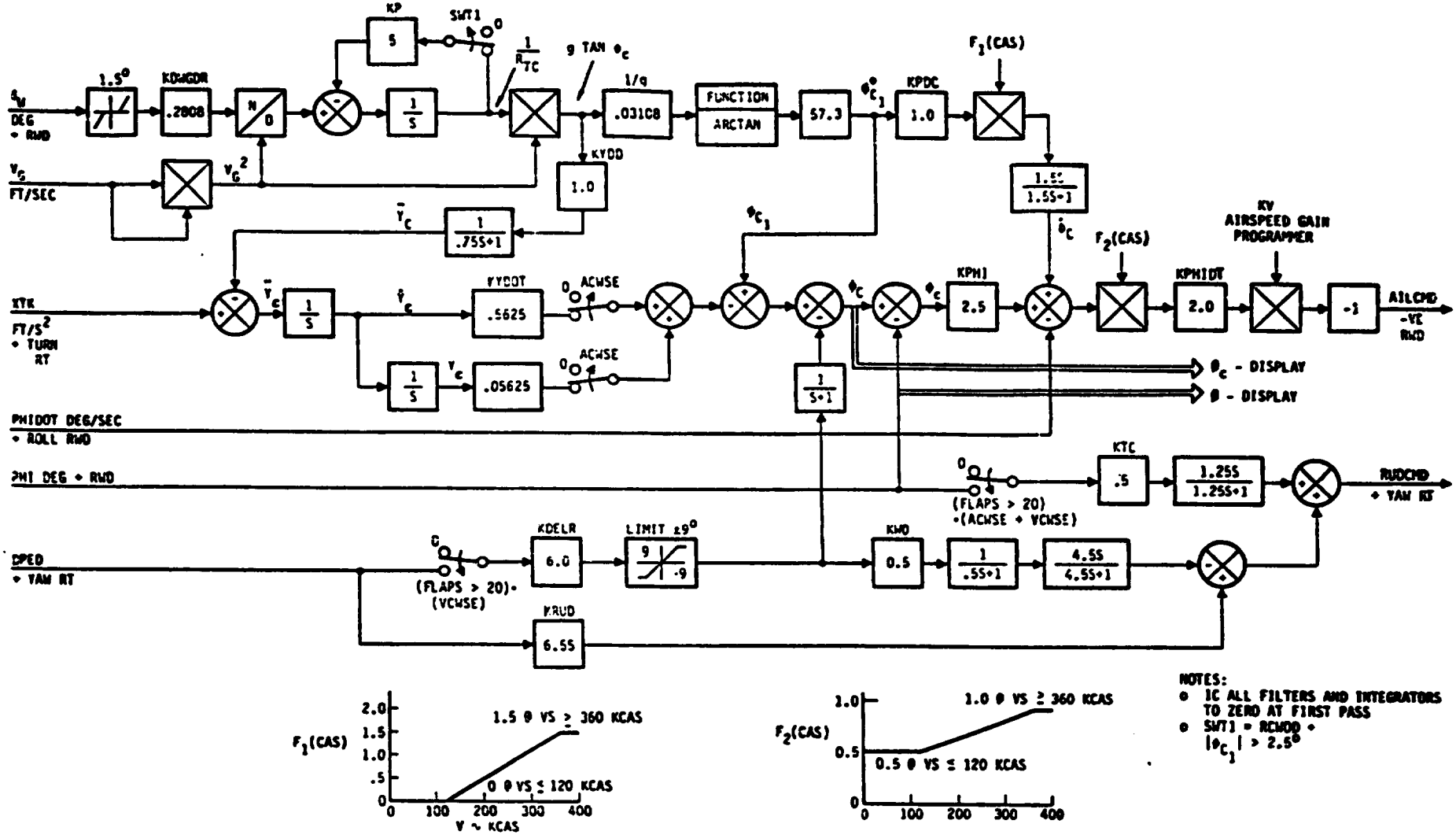

Figure 3. - Configuration B lateral CWS system (from [4]).

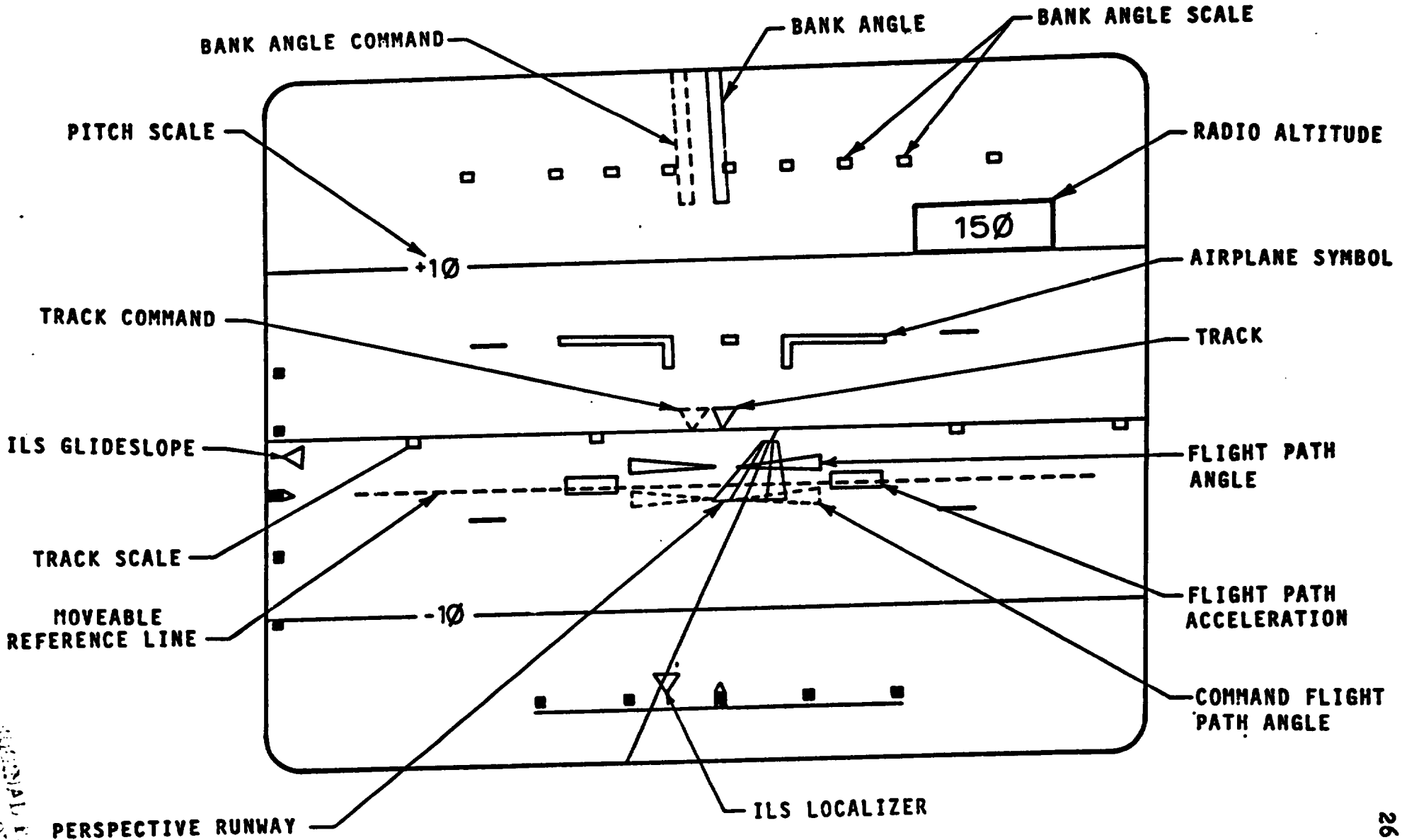

Figure 4. EADI display

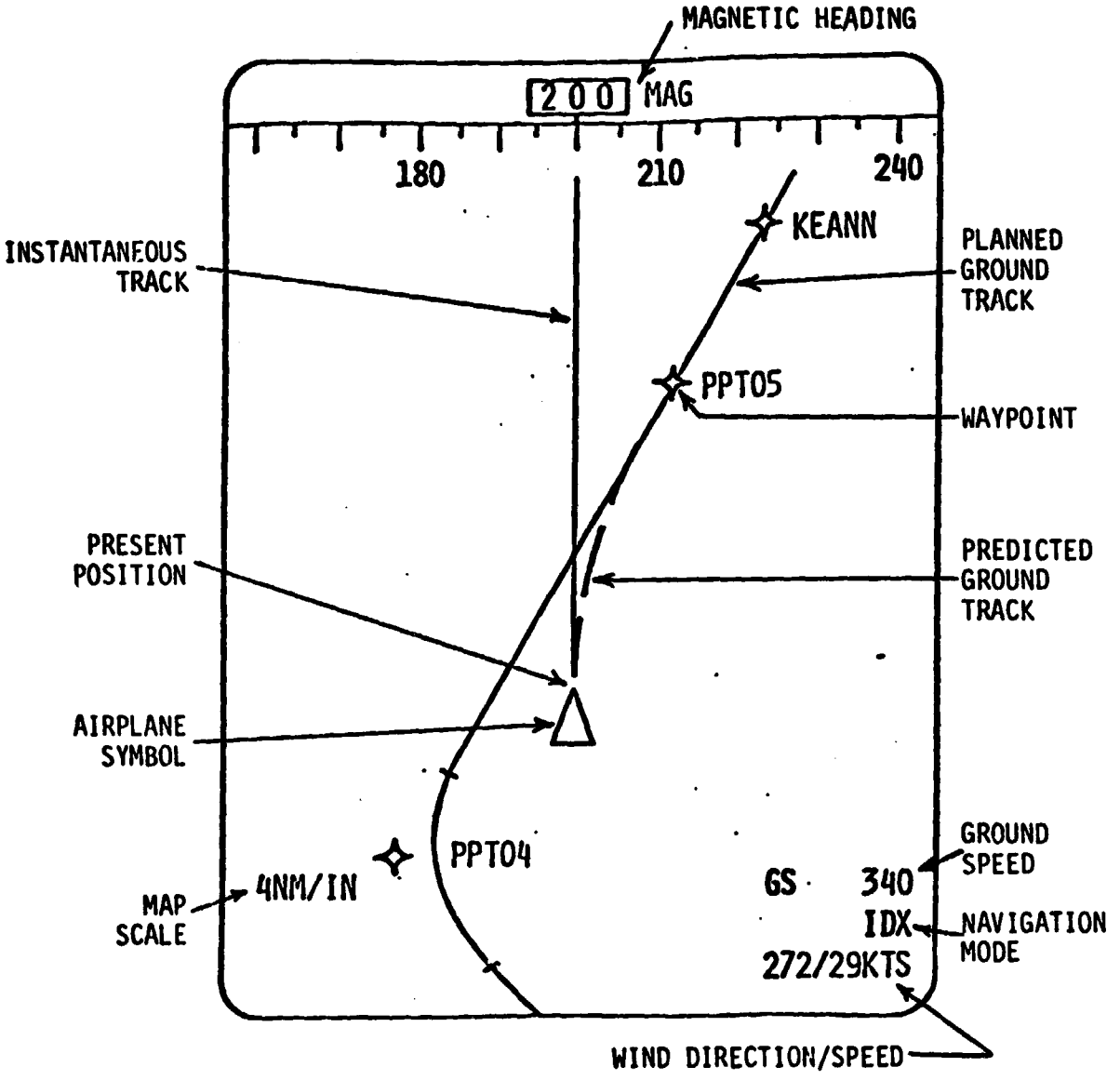

Figure 5. EHSI display.

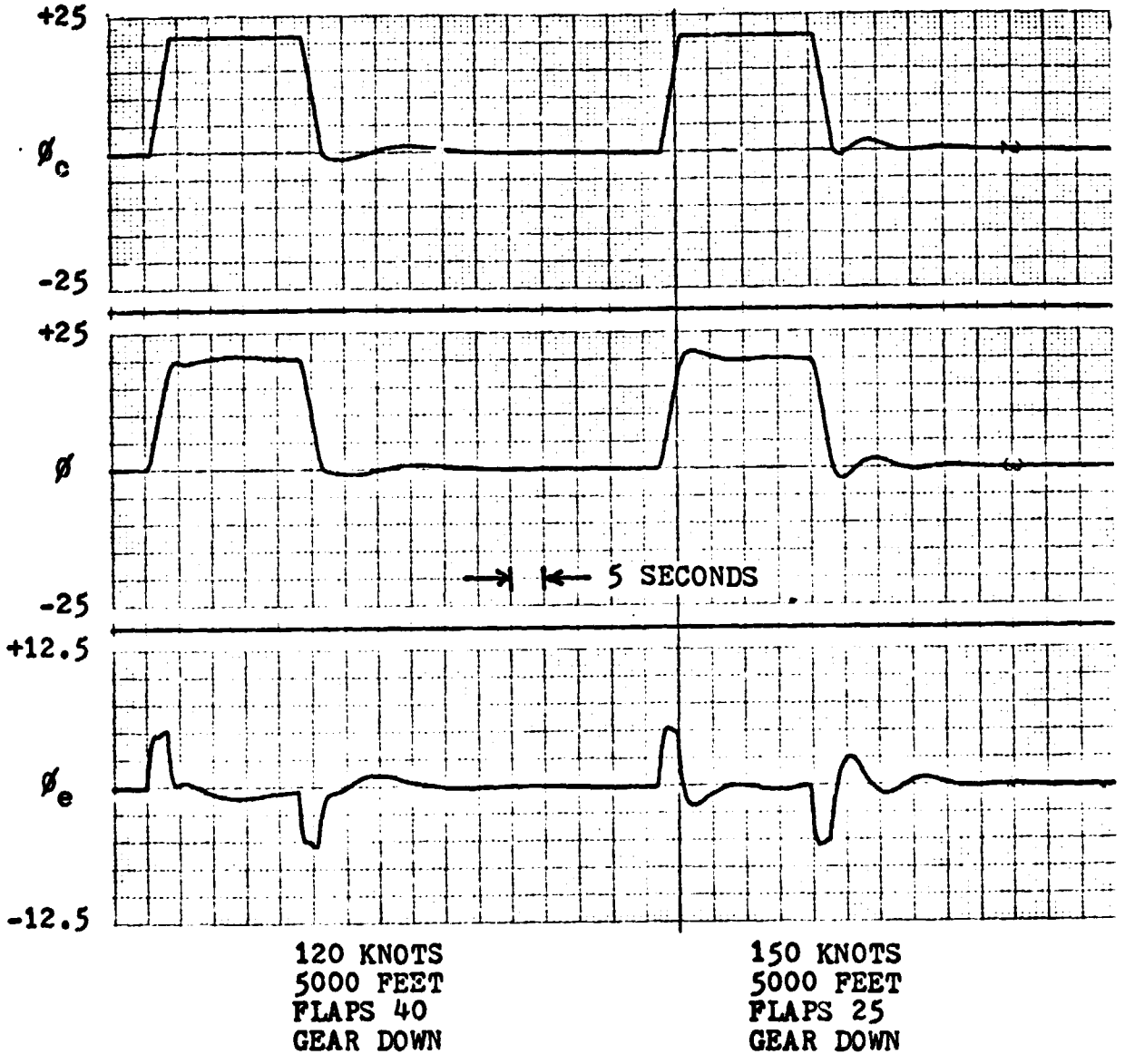

Figure 6. Configuration A roll response from RTS.

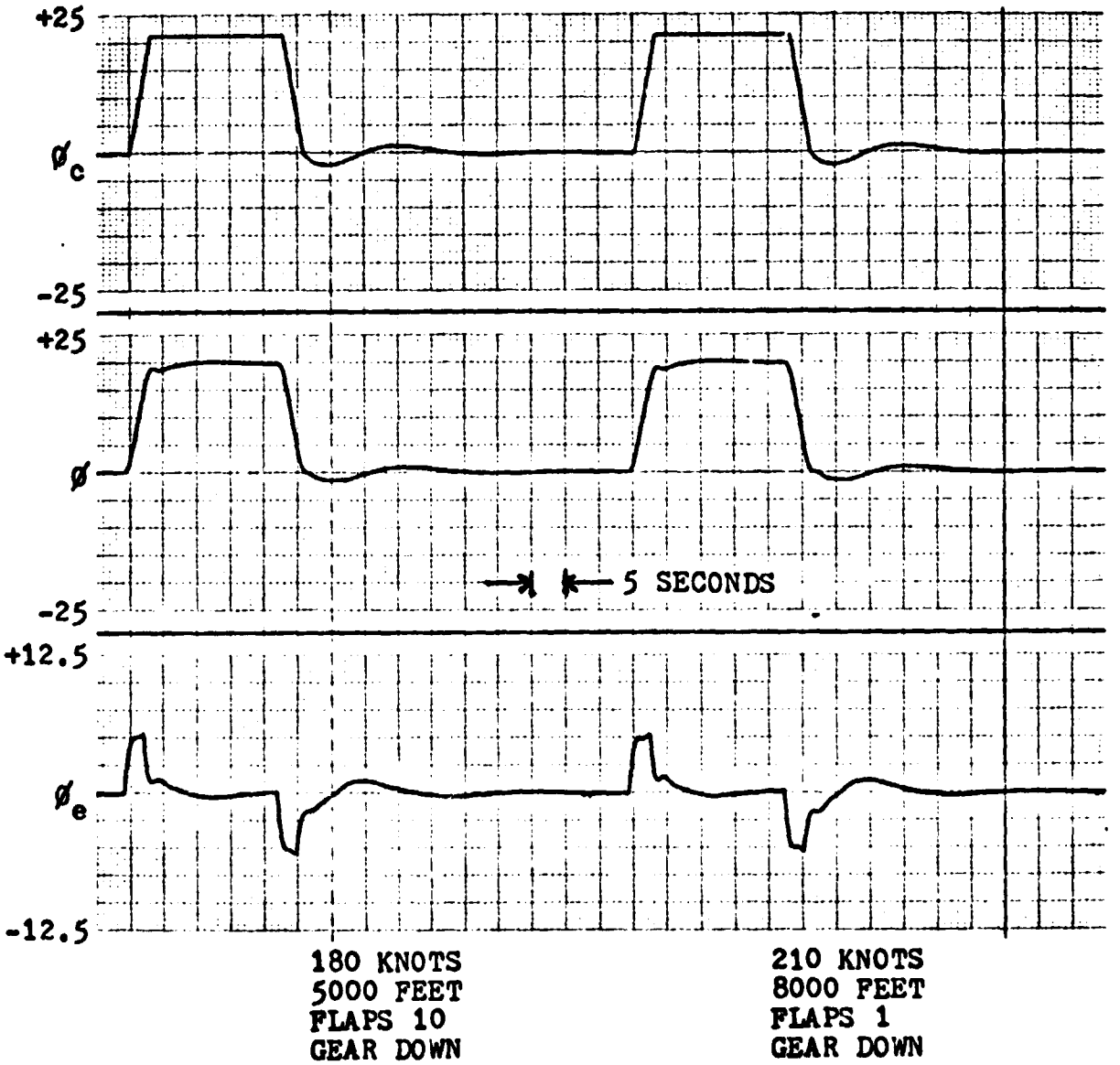

Figure 6. (continued)

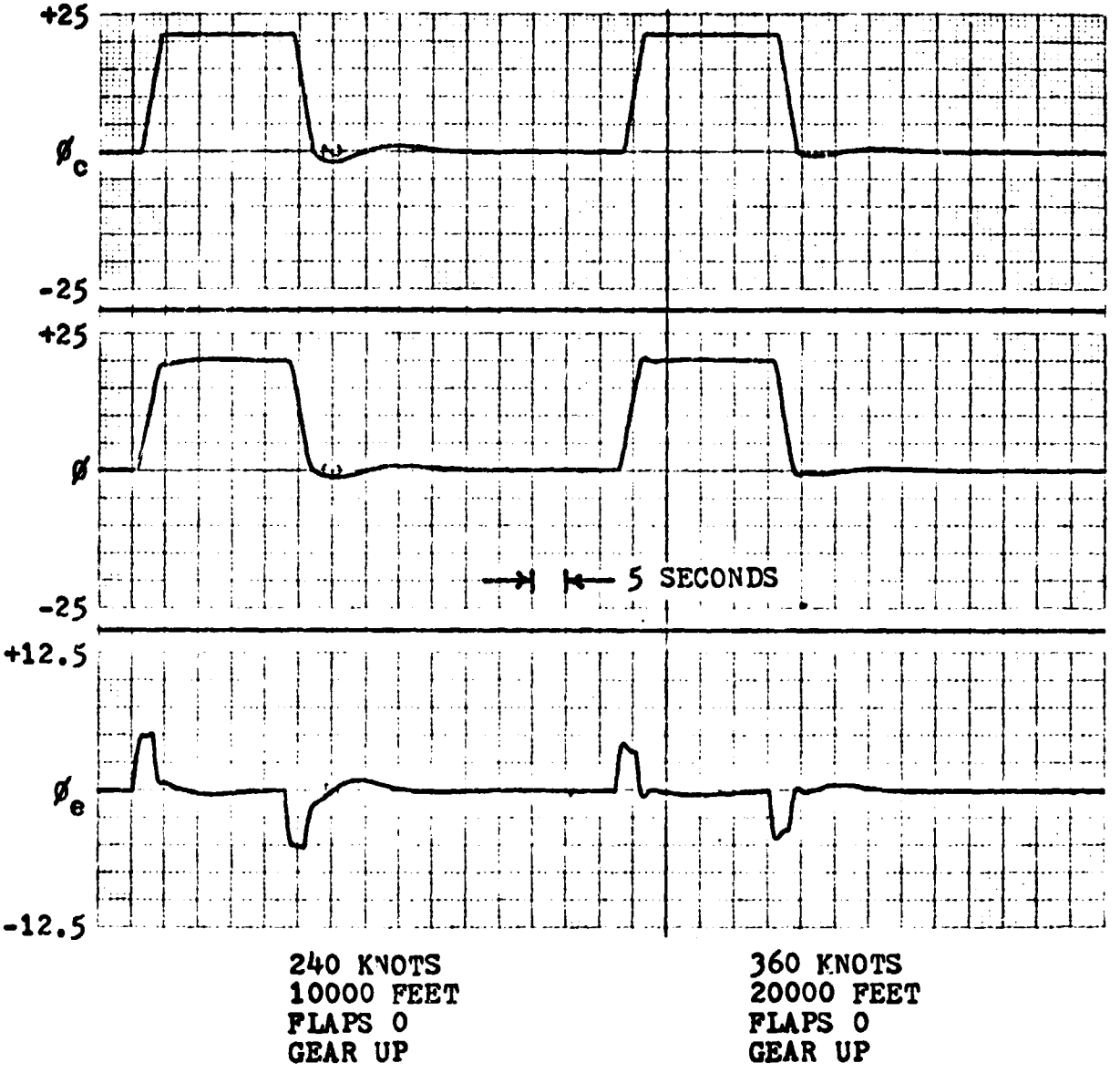

Figure 6. (continued)

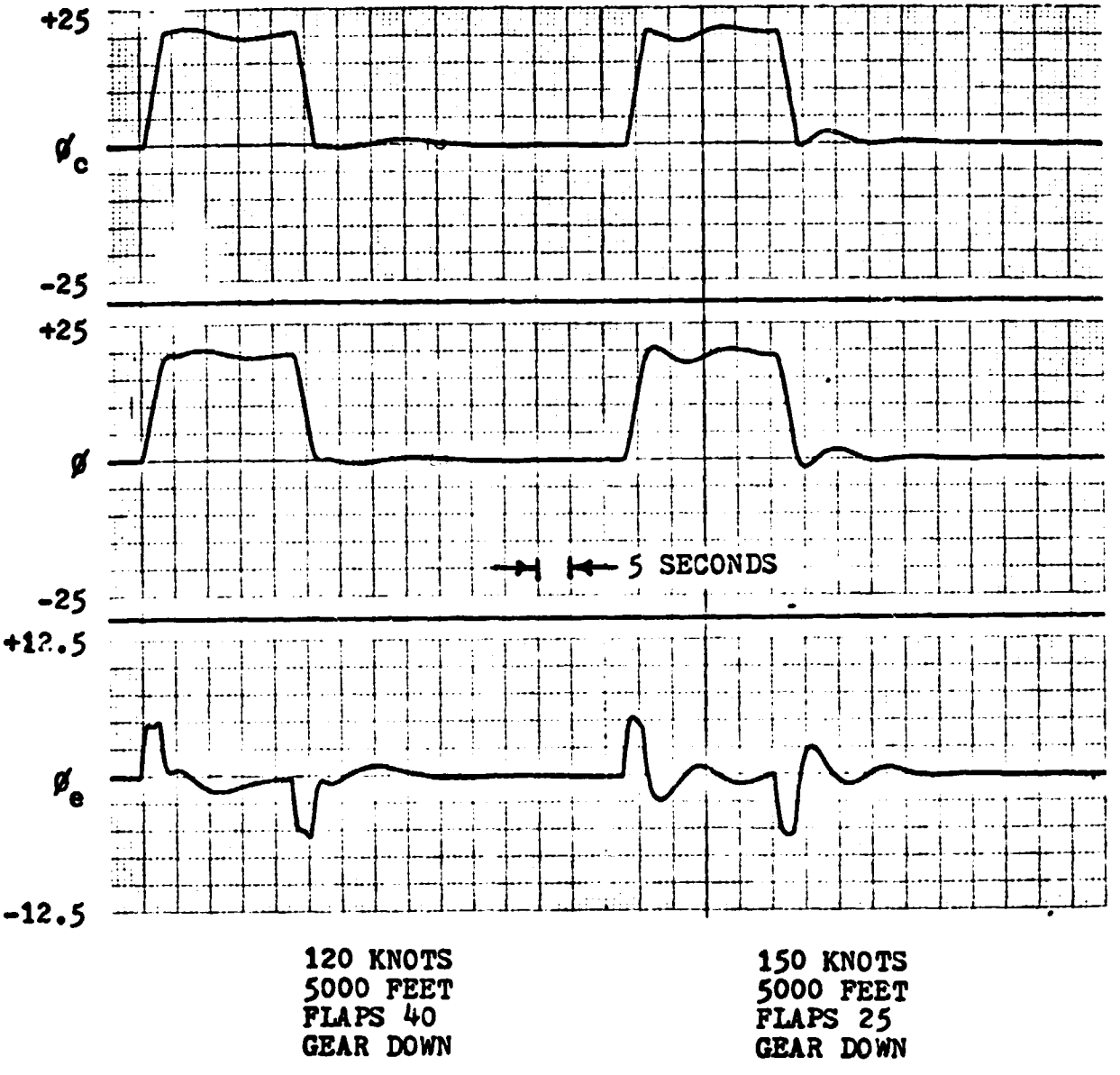

Figure 7. Configuration B roll response from RTS.

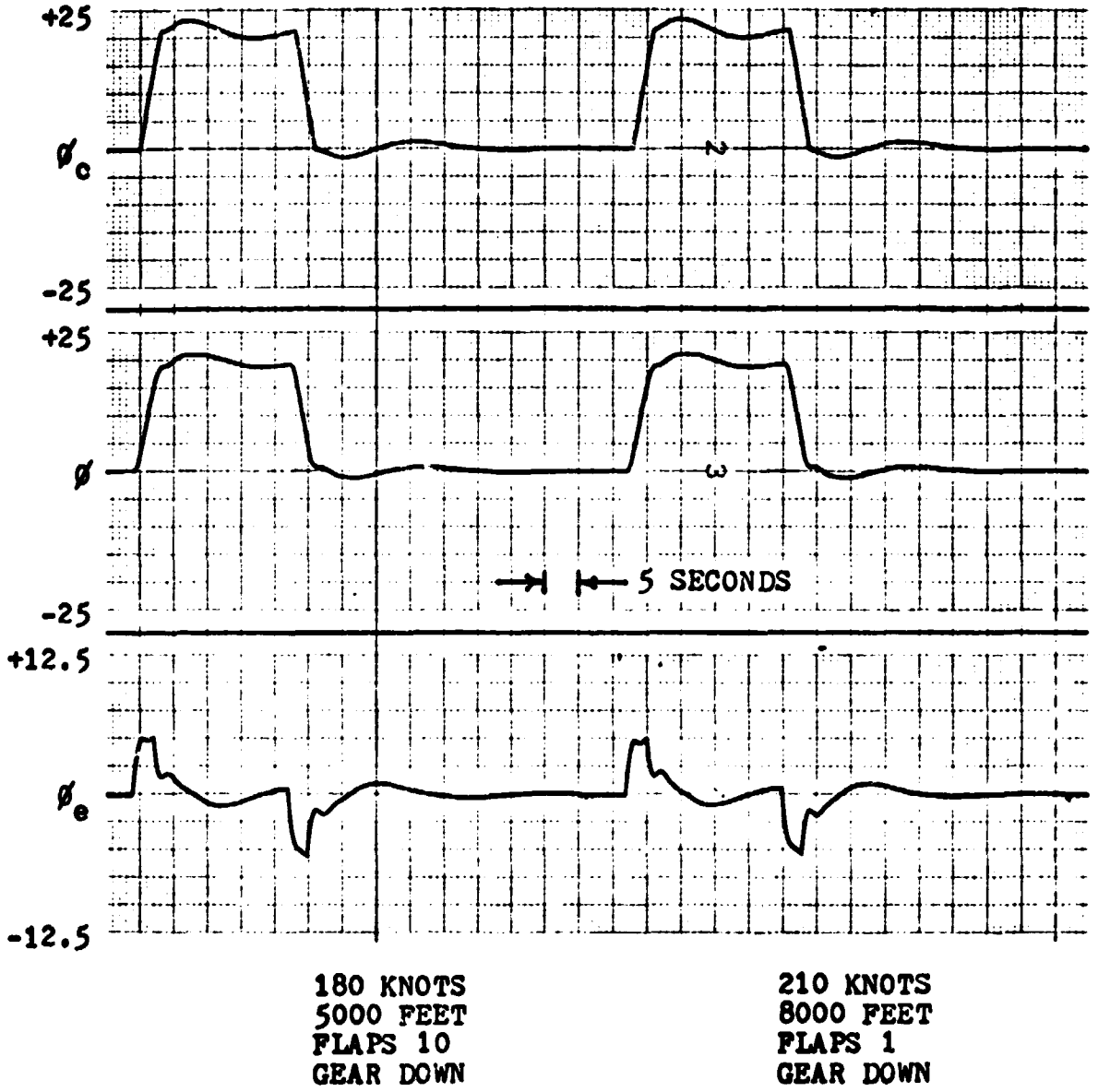

Figure 7. (continued)

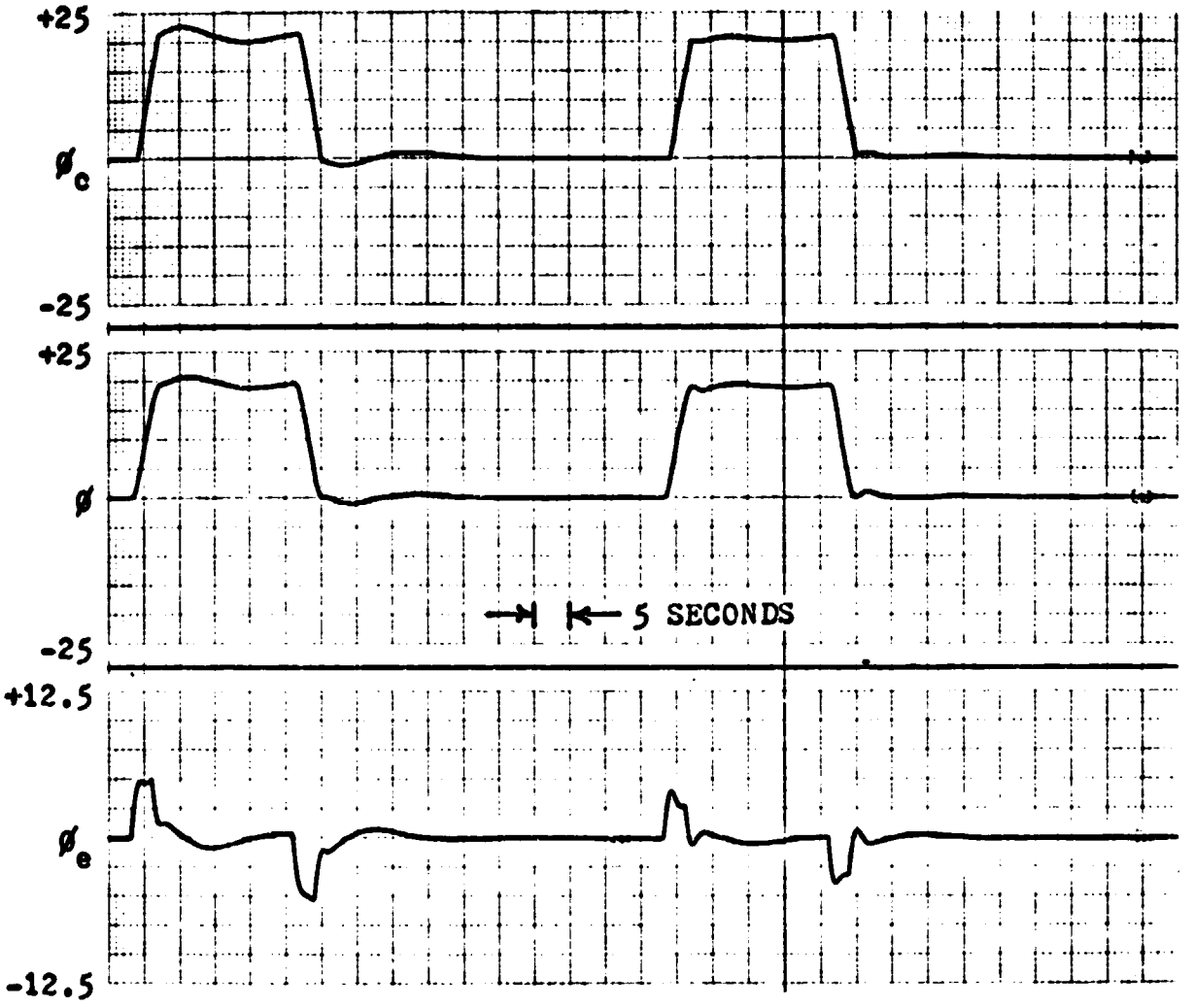

Figure 7. (continued)

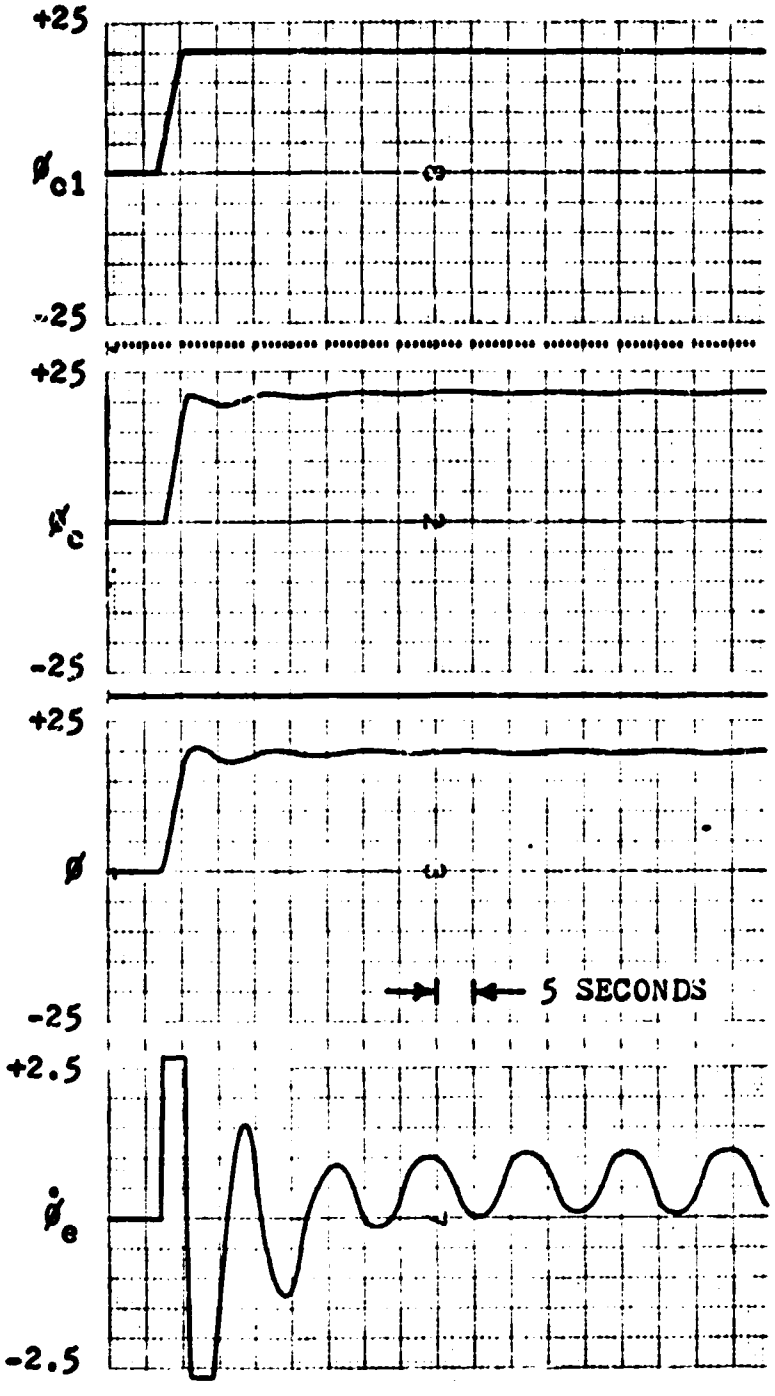

Figure 8. (a) Configuration B roll response with original servo models.

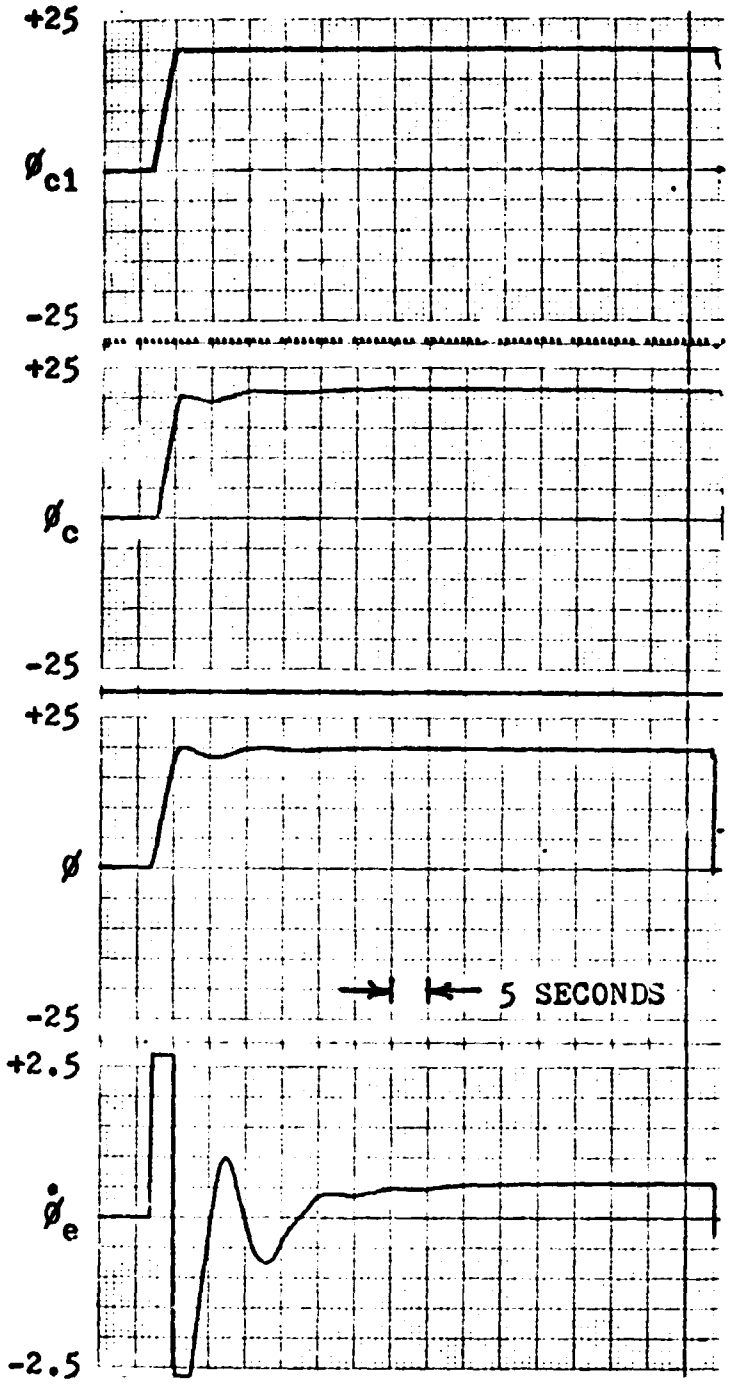

Figure 8. (b) Configuration B roll response with updated servo models.

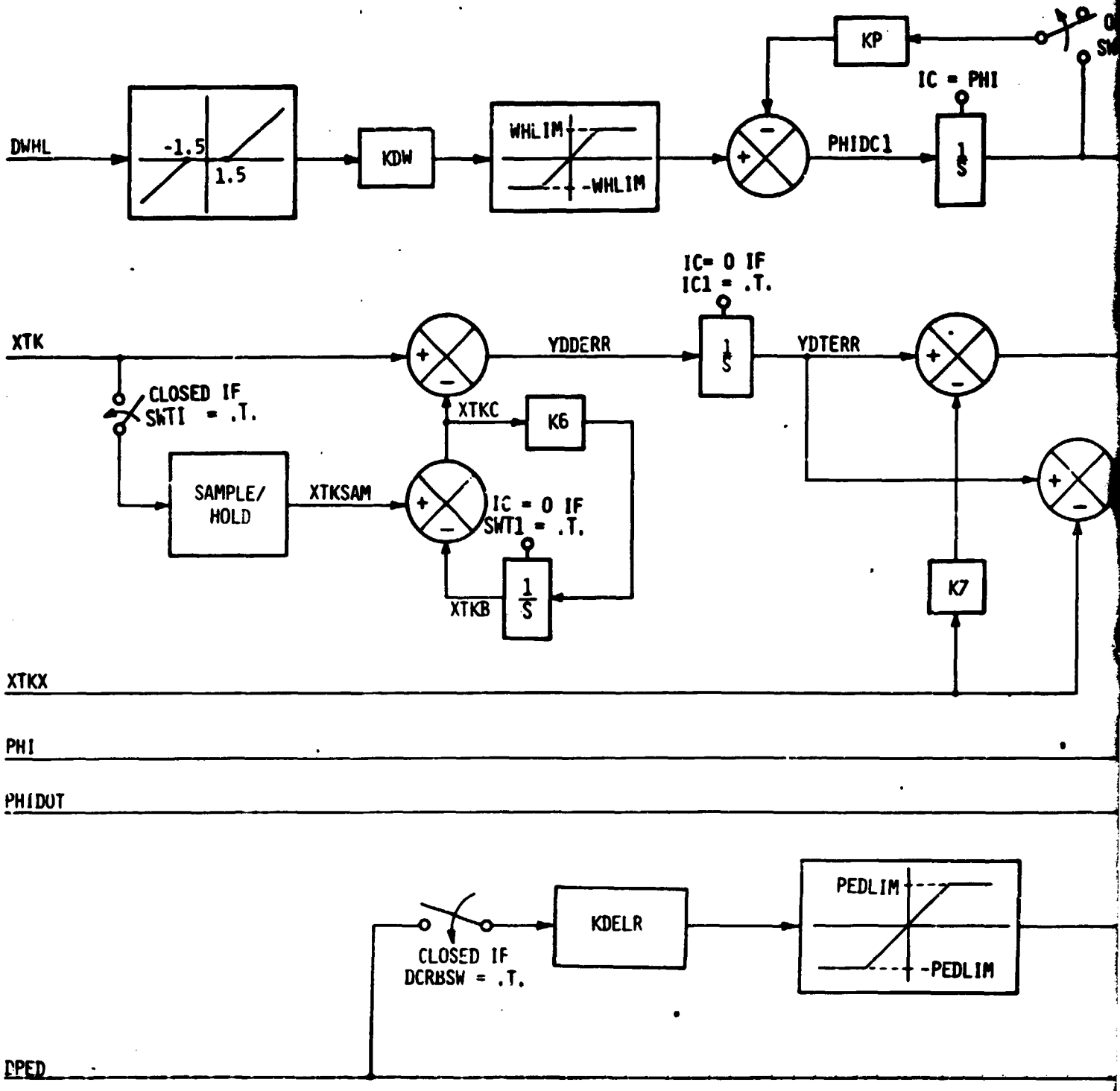

FOLDOUT FRAME

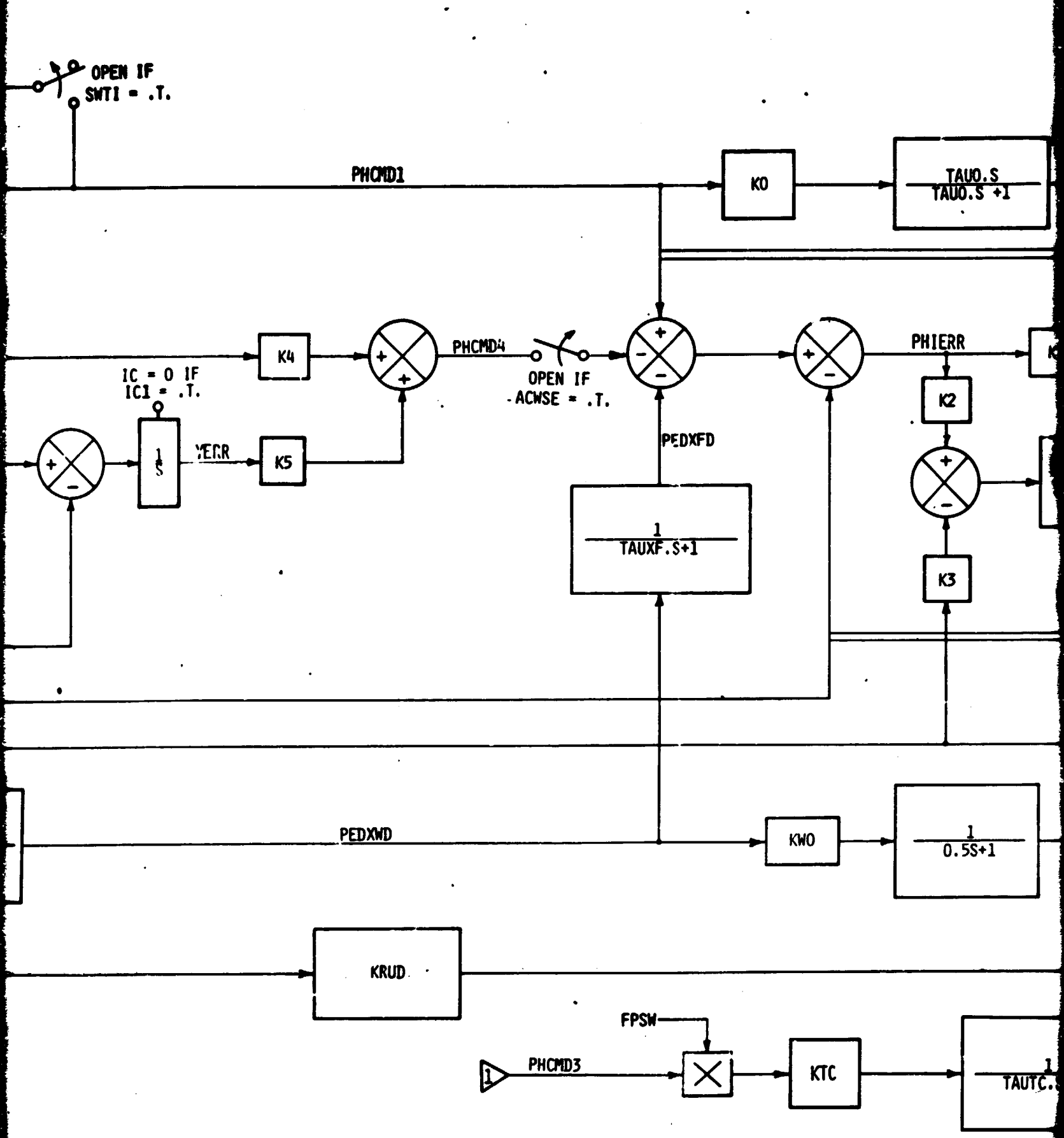

FOLDOUT FRAME 2

FIGURE 9. LATERAL VELOCITY CWS CONTROL LAW CO

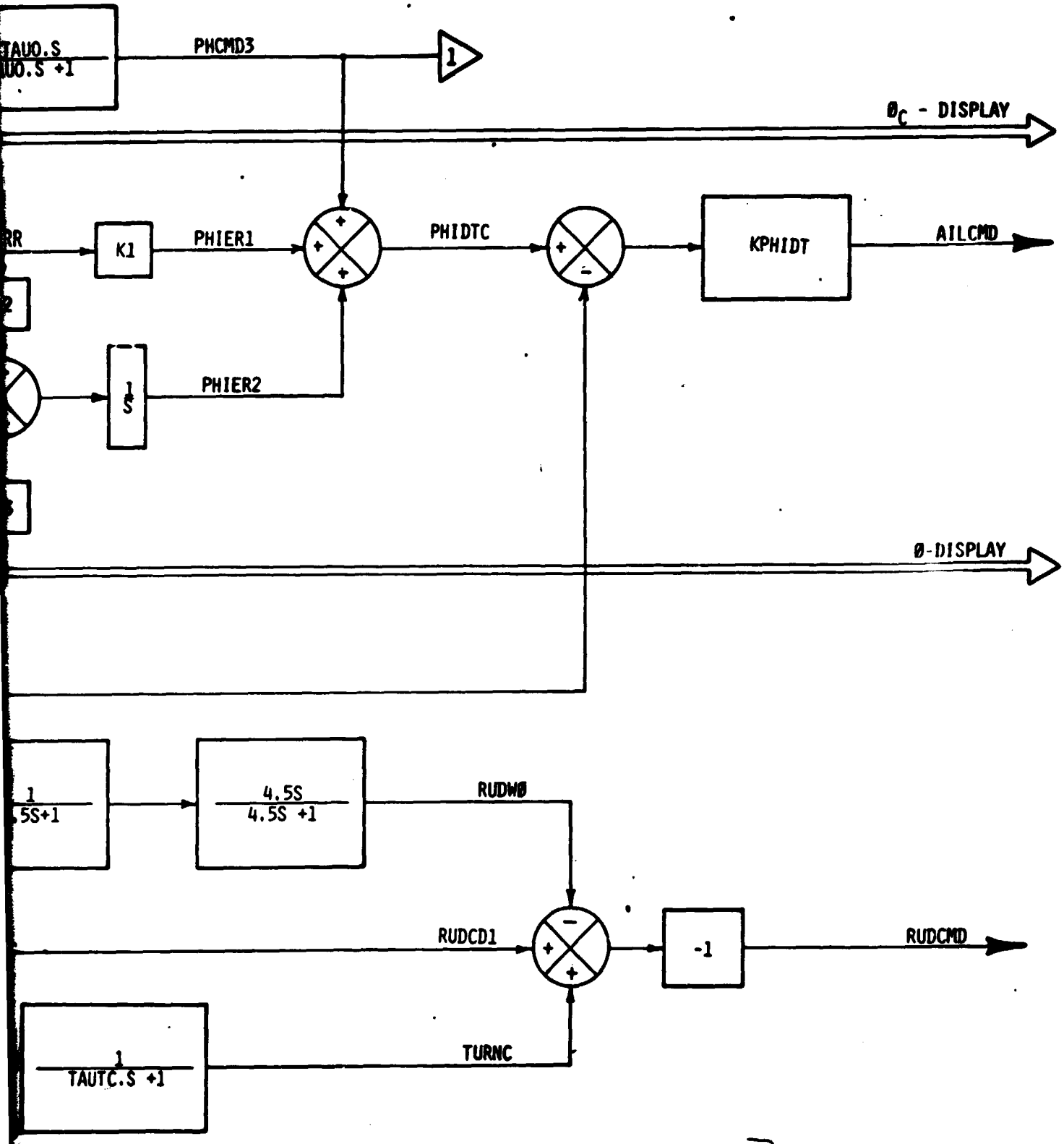

FOLDOUT FRAME 3

TROL LAW CONFIGURATION C.

ϕ_C - DISPLAY

AILCMD

Ø-DISPLAY

RUDCMD

NOTES:

A. ALL INTEGRATORS AND FILTERS ARE INITIALIZED TO ZERO EXCEPT AS INDICATED.

B. SEE FIGURE 10 FOR THE SUBMODE SWITCHING VARIABLES SWTI AND IC1.

C. SEE FIGURES 11 AND 12 FOR THE RELATIVE TRACK ANGLE COMMAND SIGNAL XTKX.

D. DCRDSW = (FLAPS.GT.25.) .AND. VCWSE.

E. NOMINAL GAINS, TIME CONSTANTS, AND LIMITS:

KDW	= 0.5	KDELR	= 2.5
KP	= 5.0	TAUXF	= 1.0
TAUO	= 0.5	KWØ	= 0.5
KO	= 1.4	KRUD	= 6.55
K1	= 0.5	KTC	= 1.0
K2	= 0.7	TAUTC	= 1.0
K3	= 0.5	WHLIM	= 10.0
K4	= 0.5	PEDLIM	= 5.0
K5	= 0.05	PHILIM	= 0.5 } SEE FIGURE 10.
K6	= 0.75	RØLIM	= 2.5 }
K7	= 0.6	DEGINC	= 0.5 } SEE FIGURE 12.
KPHIDT	= 5.0	RADINC	= 8.7266×10^{-3} }

F. FPSW GAIN SCHEDULE

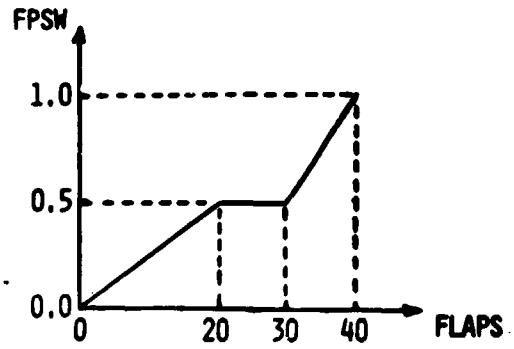

FOLDOUT FRAME 4

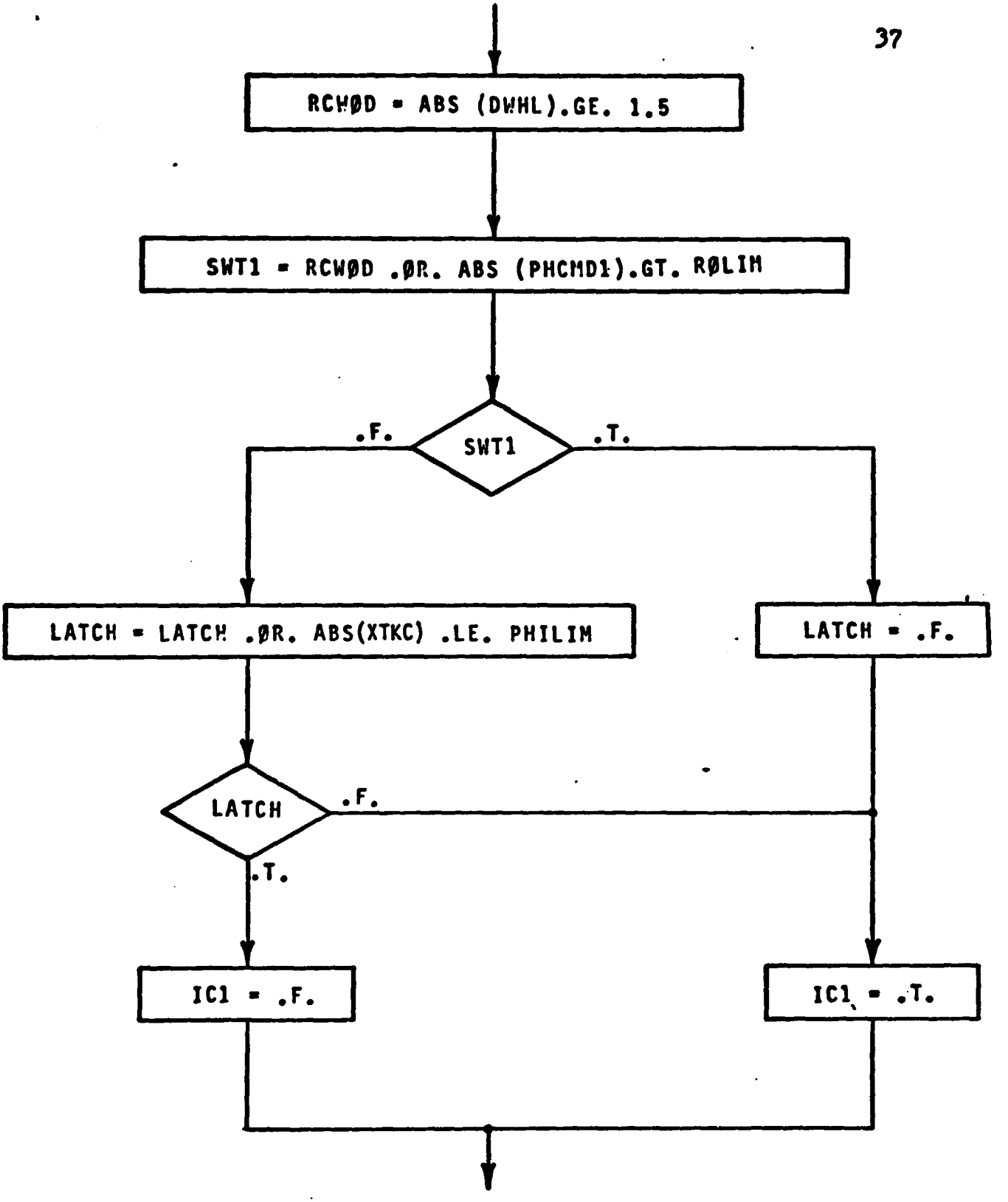

Figure 10. Configuration C submode switching logic.

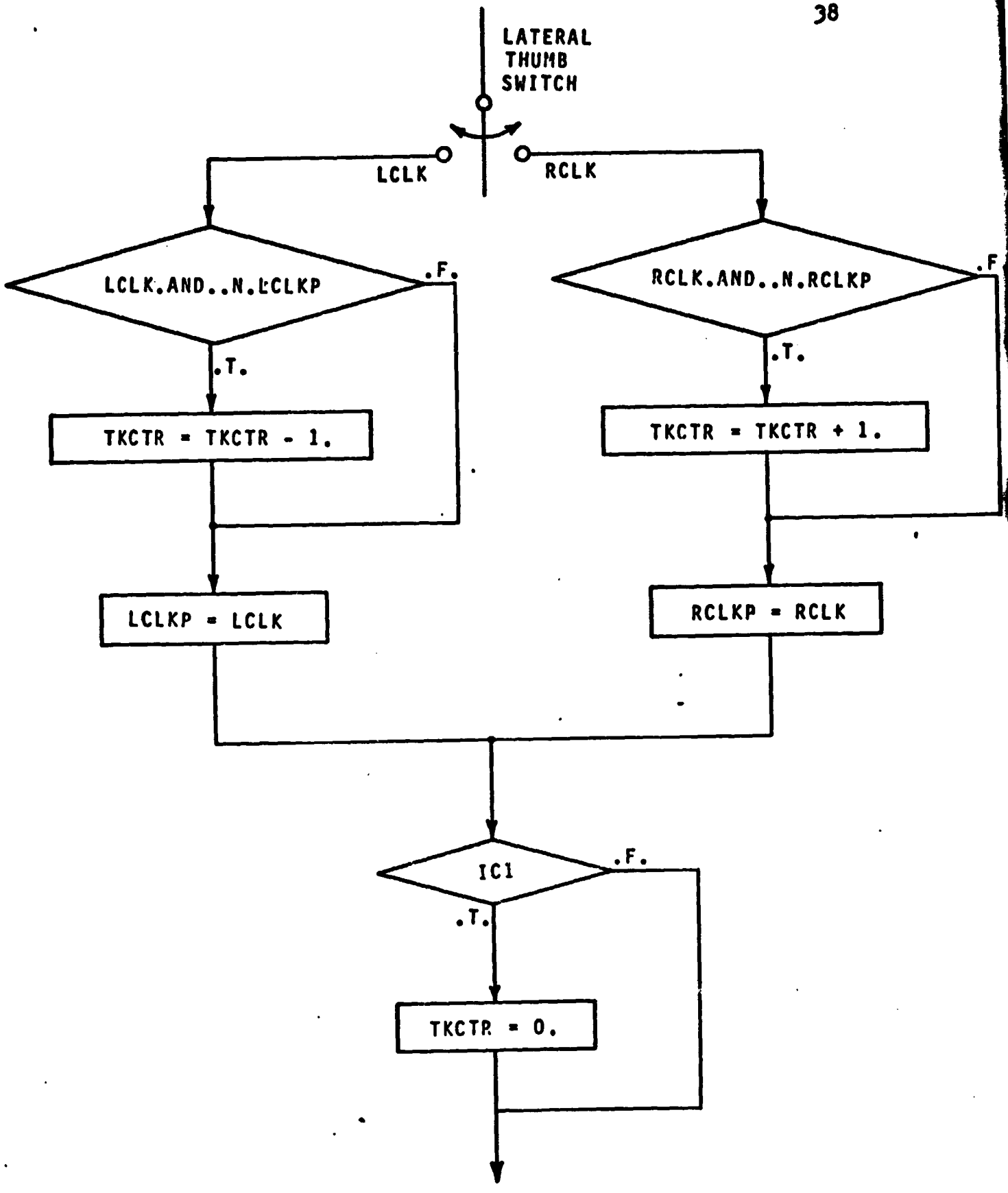

Figure 11. Lateral thumb switch logic.

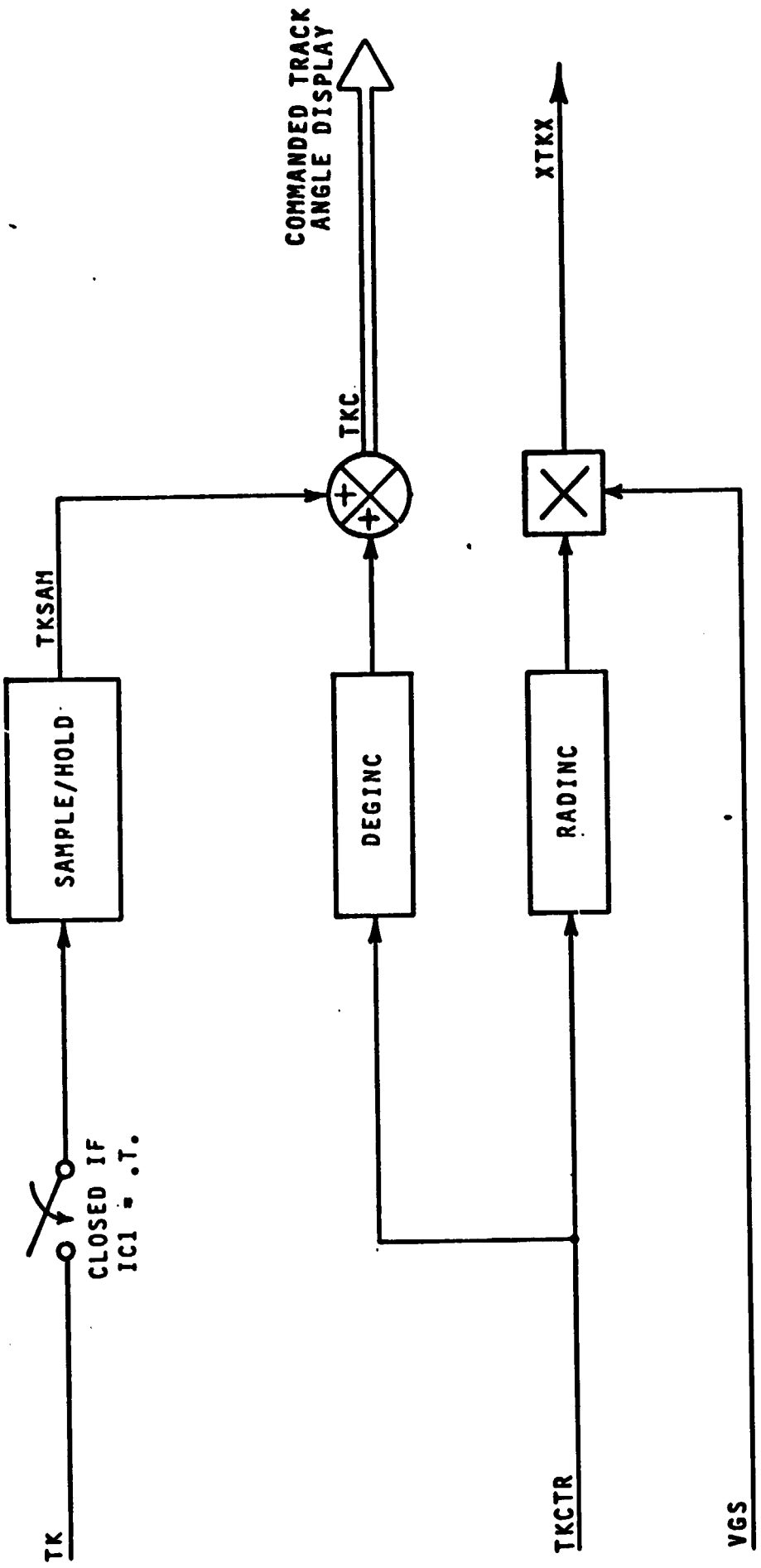

Figure 12. Relative track angle command processing.

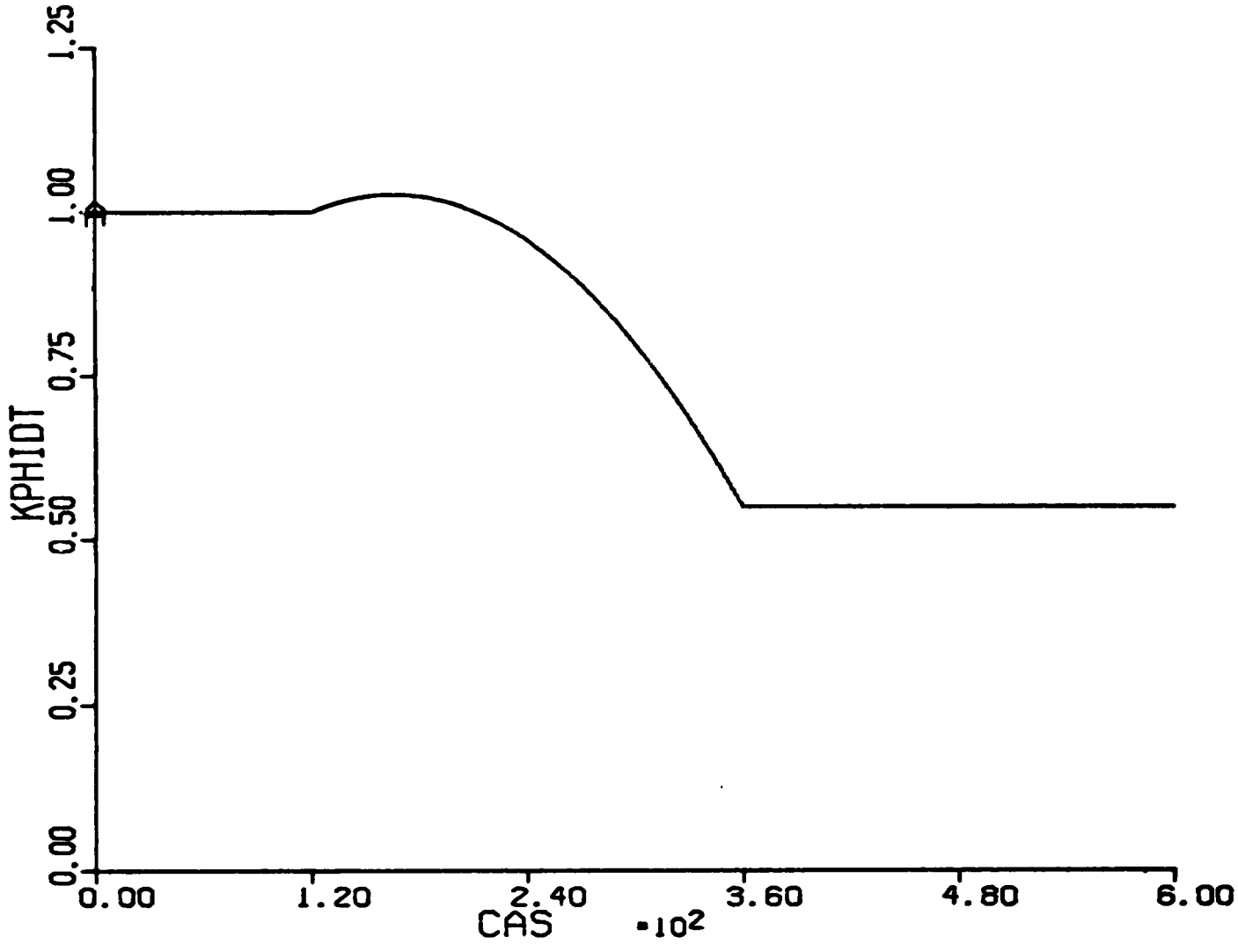

Figure 13. Effective KPHIDT for configuration A.

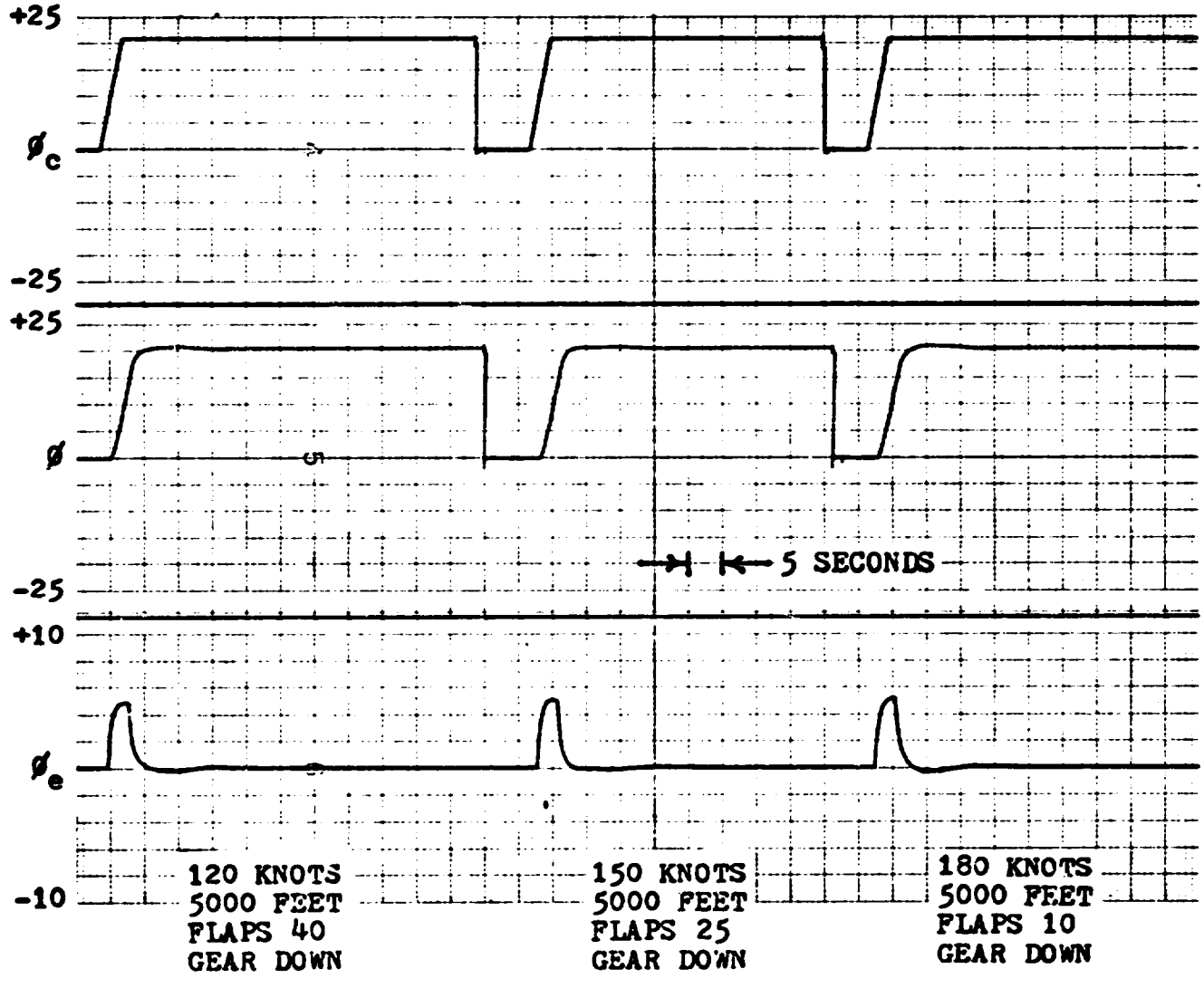

Figure 14. Configuration C attitude-hold response from RTS.

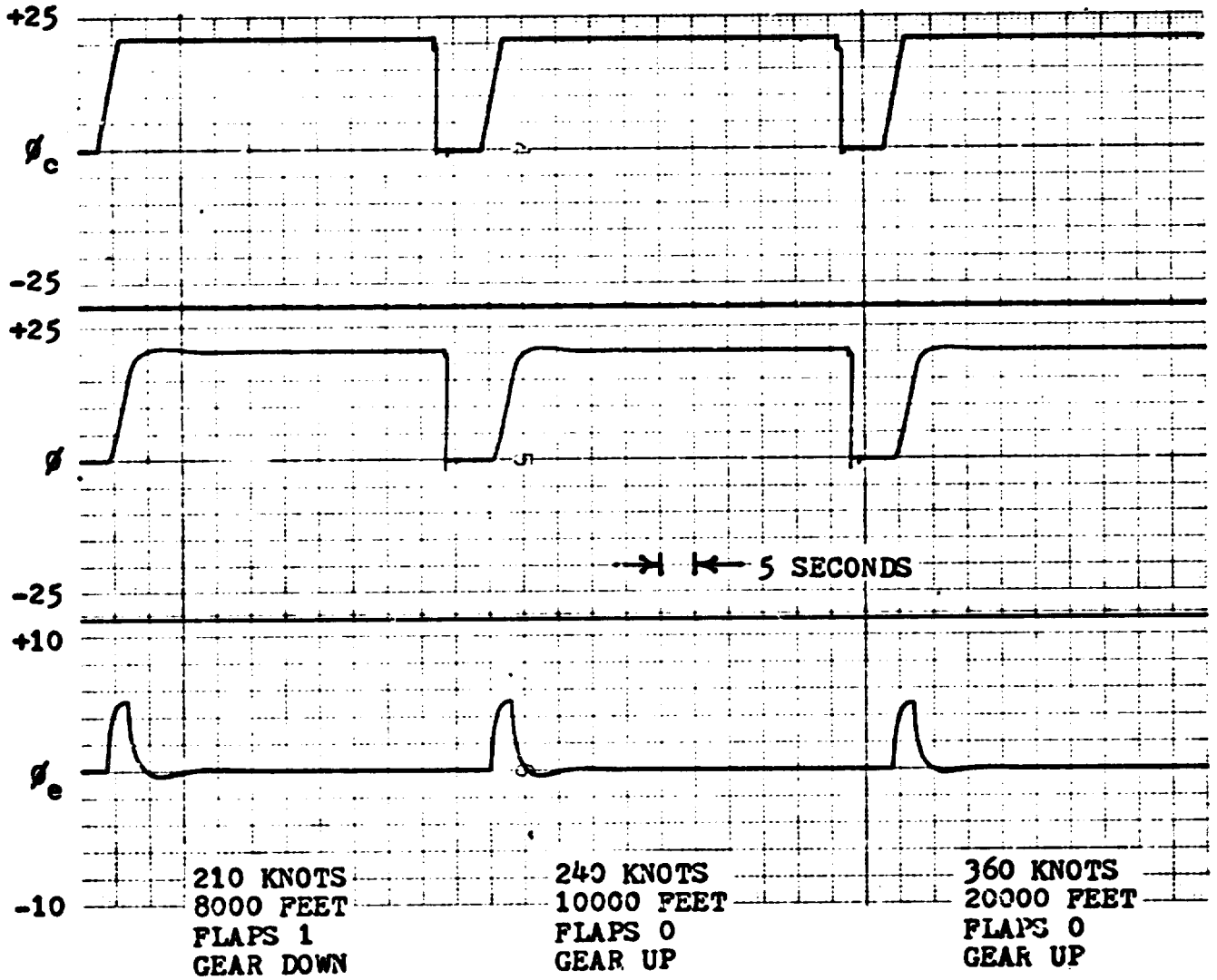

Figure 14. (continued)

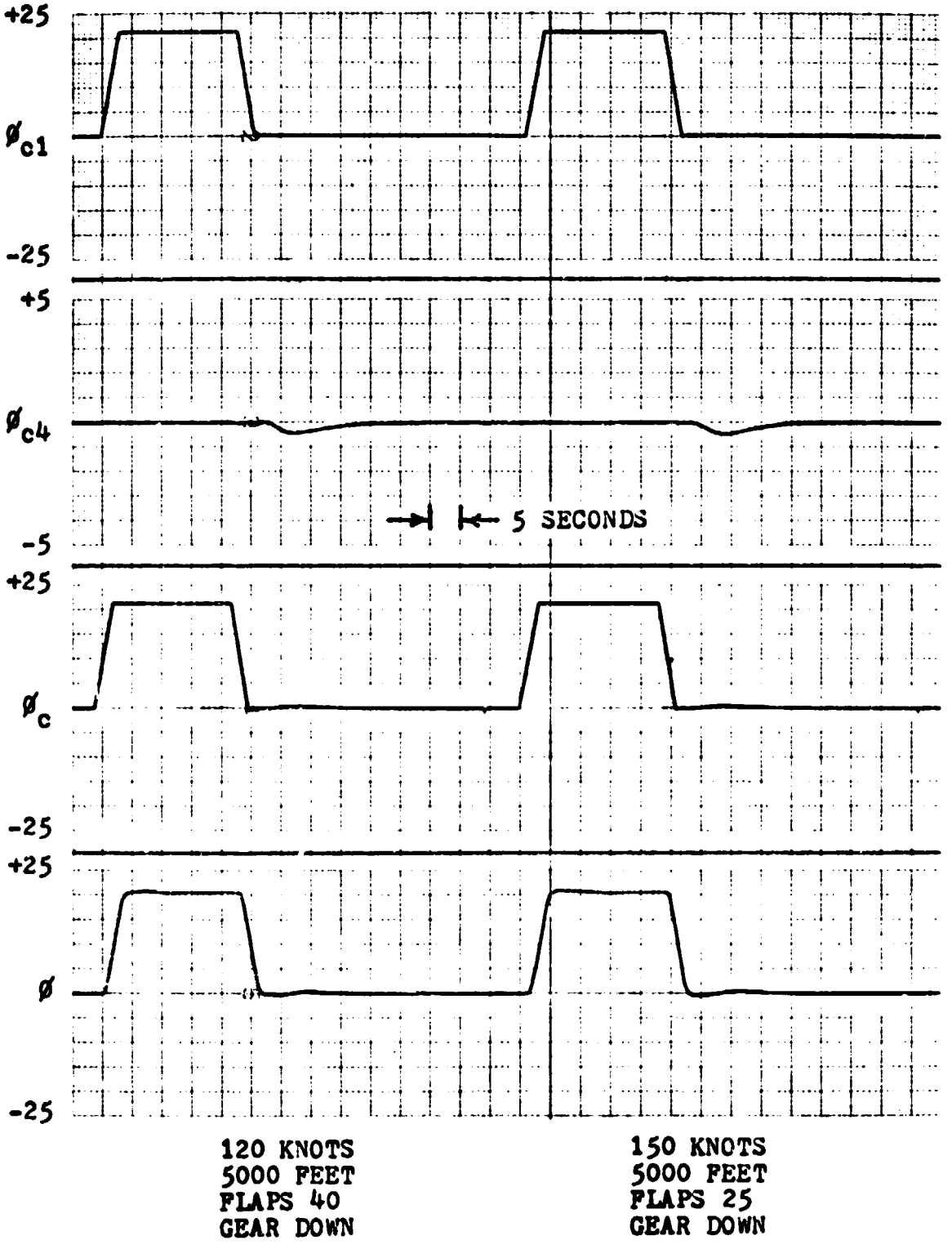

Figure 15. Configuration C track-hold response from RTS.

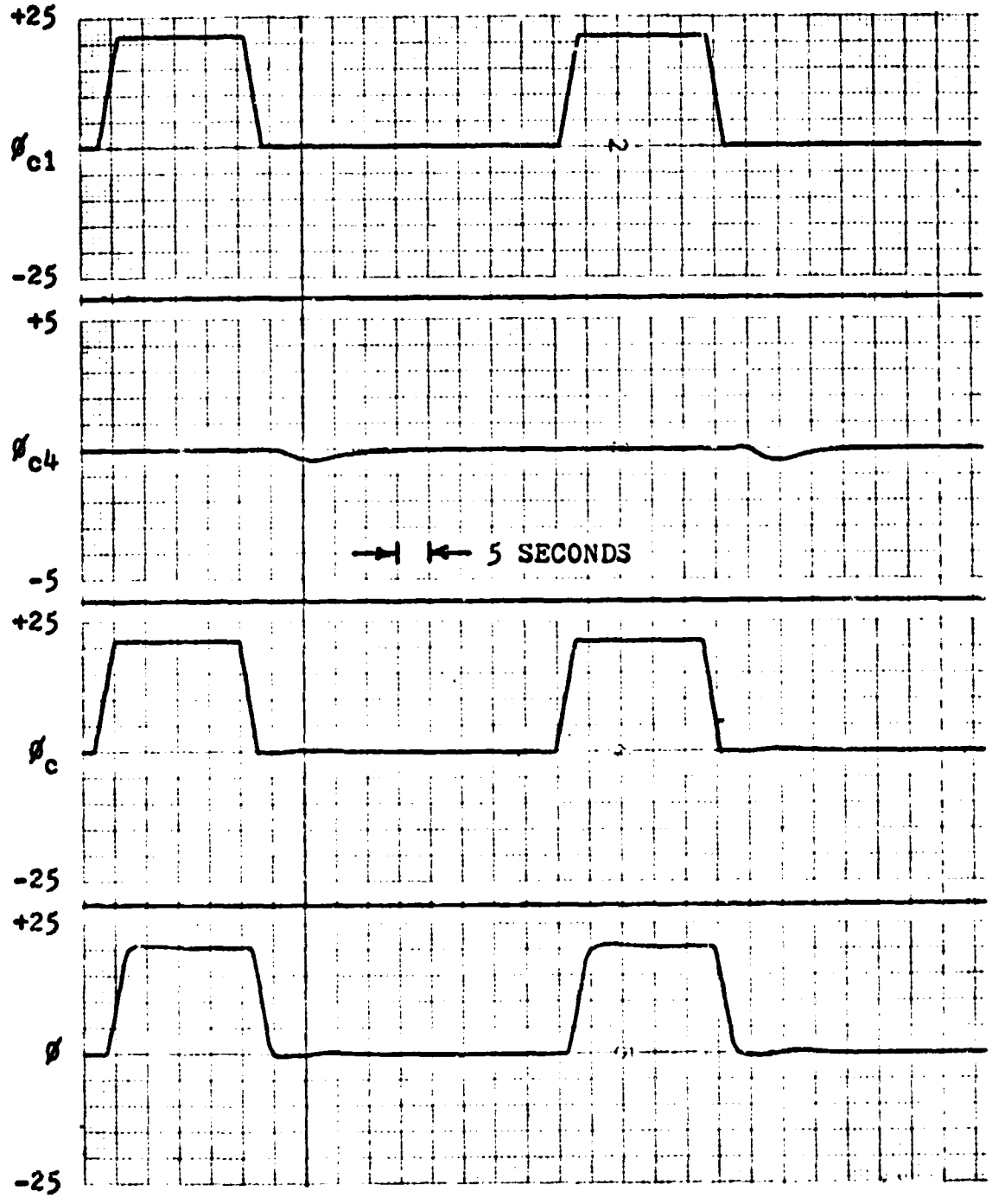

Figure 15. (continued)

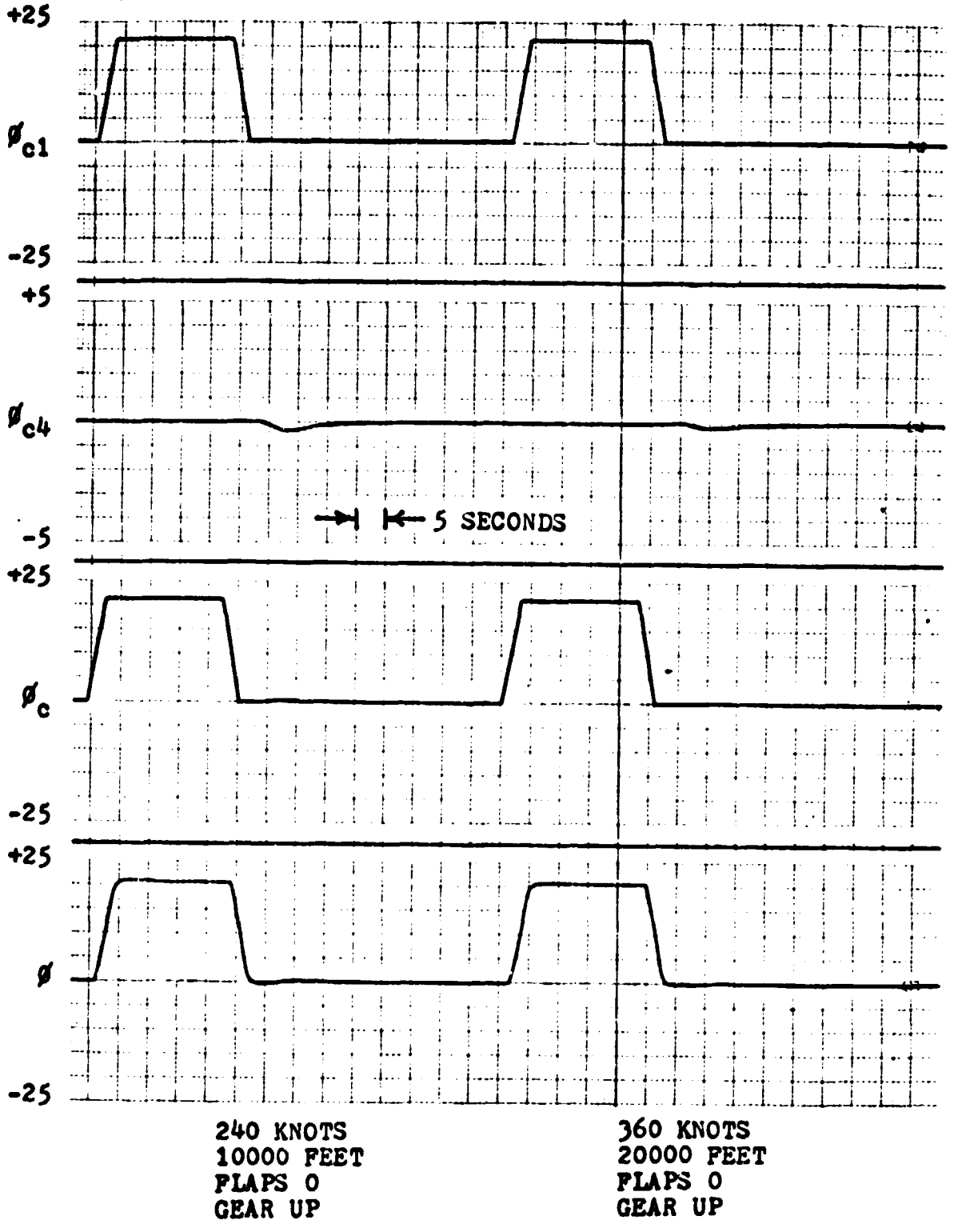

Figure 15. (continued)

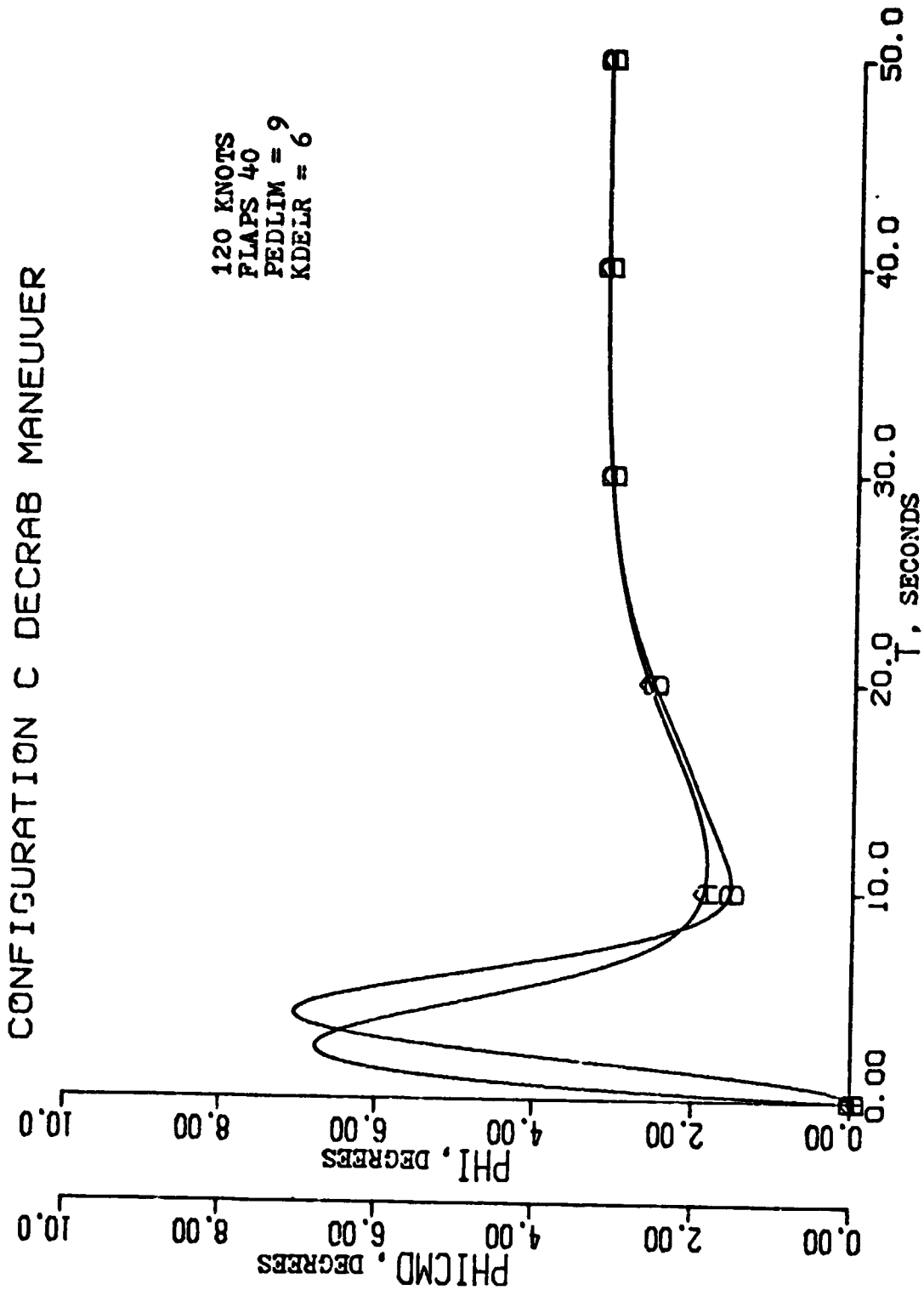

Figure 16. (a) Bank angle command (PHICMD) and bank angle (PHI) responses.

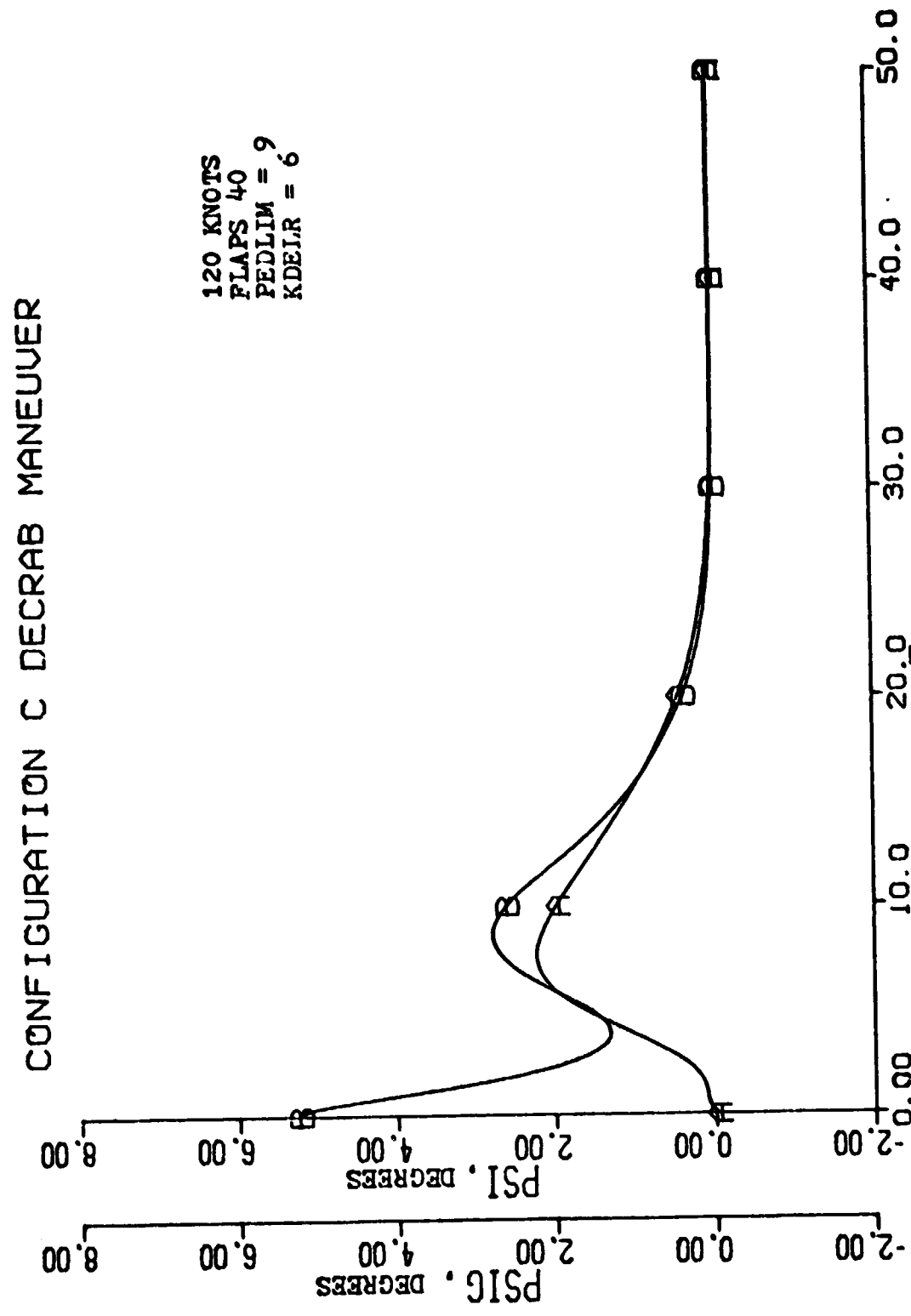

Figure 16. (b) Track angle (PSIG) and heading (PSI) responses.

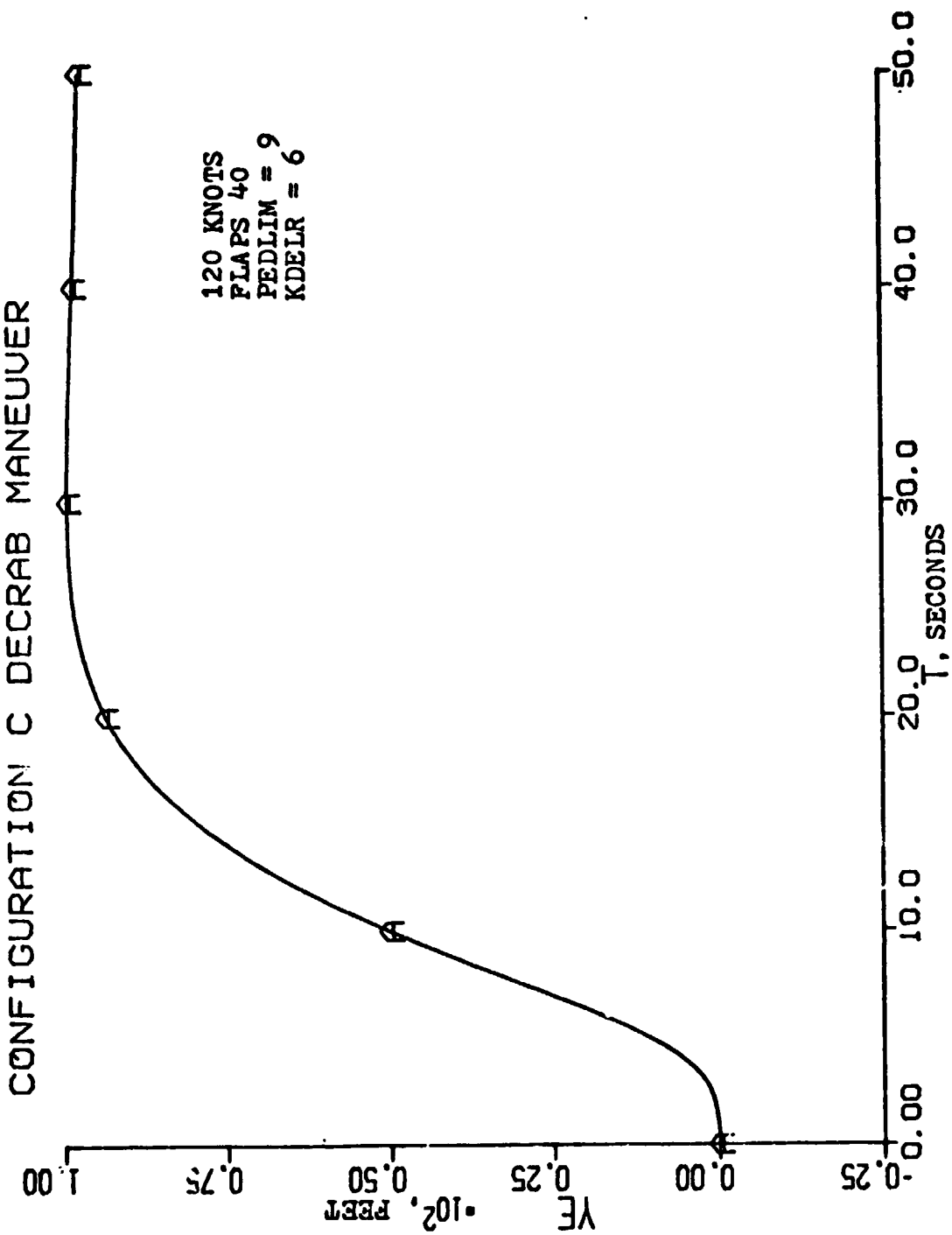

Figure 16. (c) Crosstrack error (YE) response.

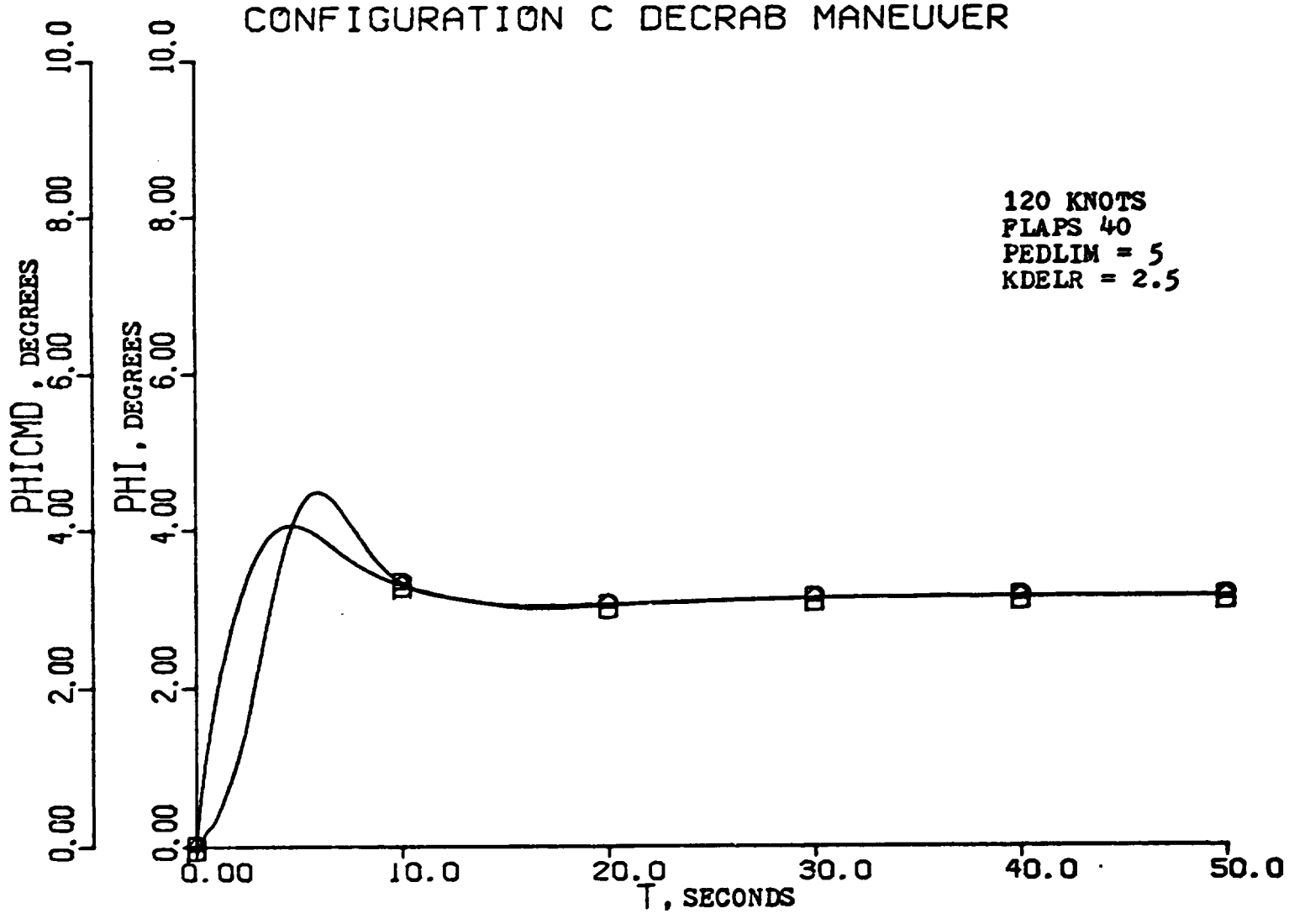

Figure 17. (a) Bank angle command (PHICMD) and bank angle (PHI) responses.

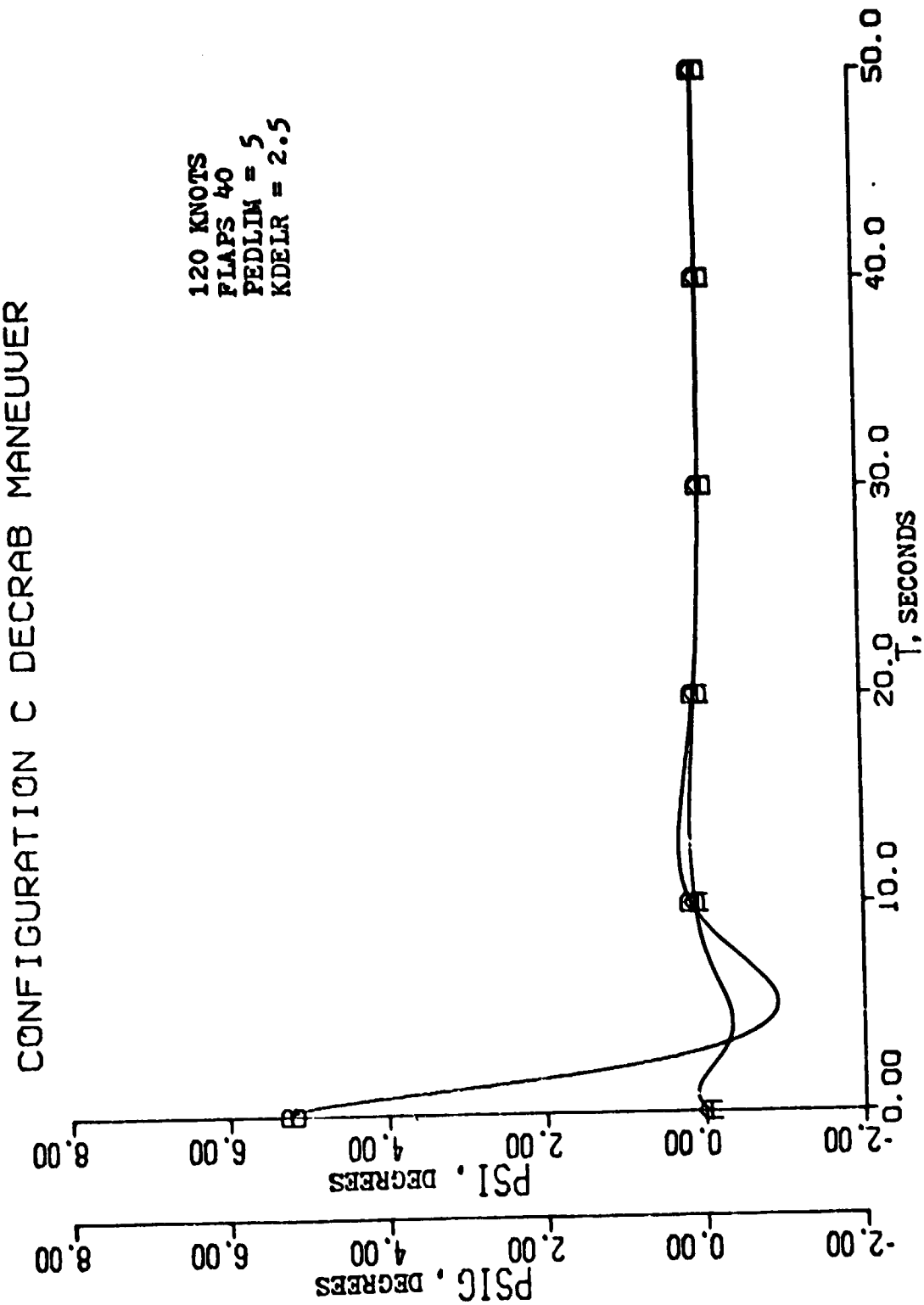

Figure 17. (b) Track angle (PSIG) and heading (PSI) responses.

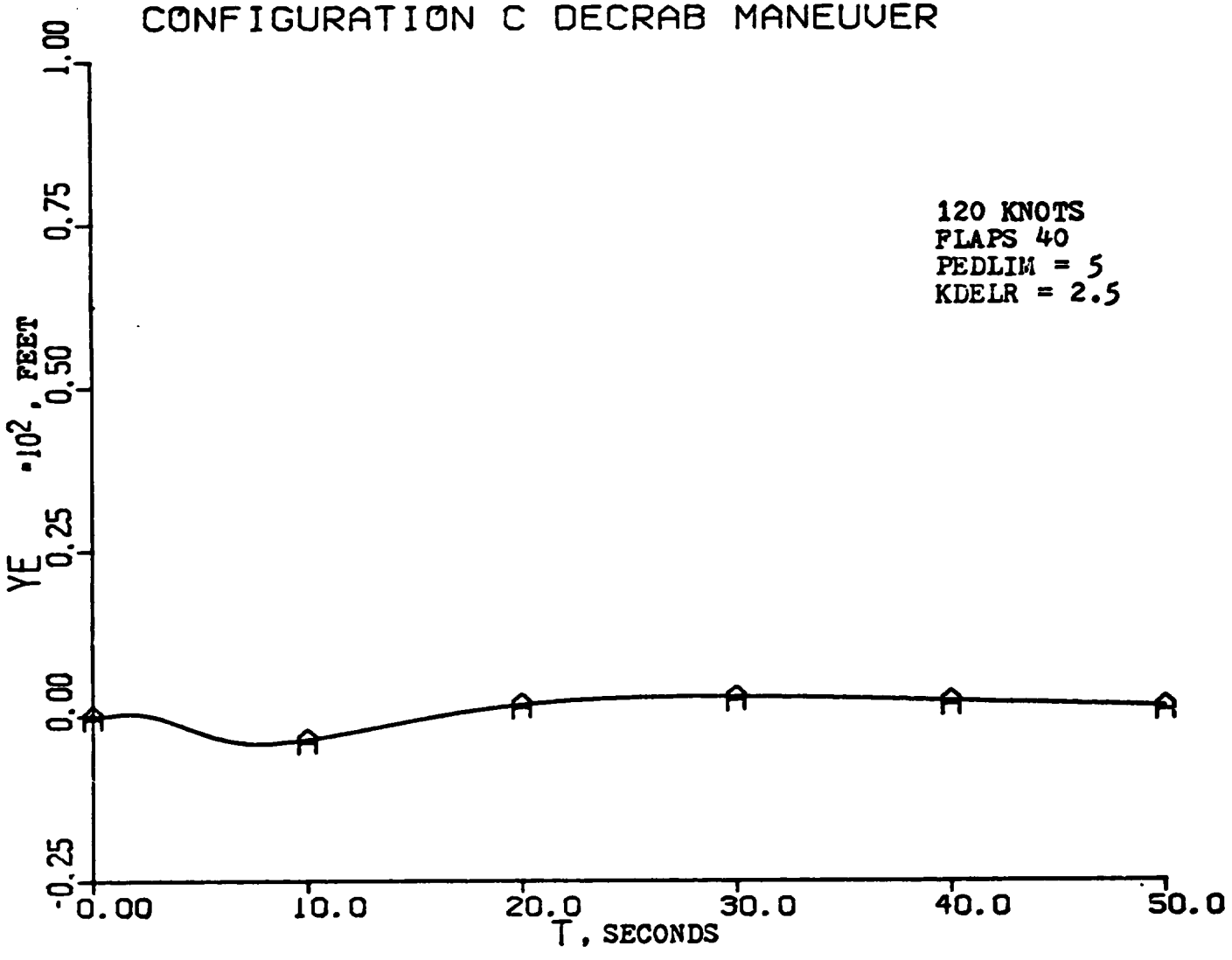

Figure 17. (c) Crosstrack error (YE) response.

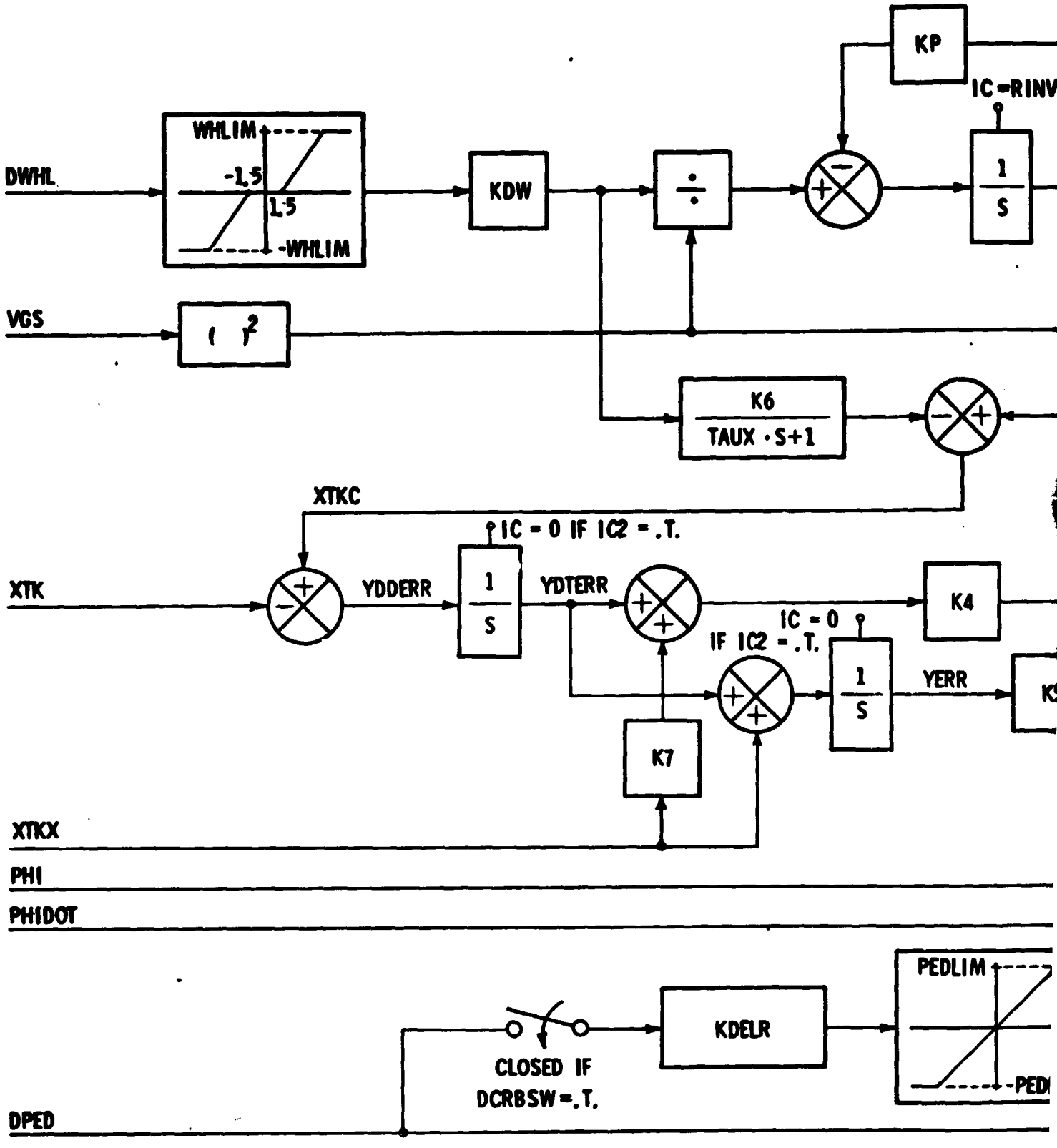

FOLDOUT FRAME

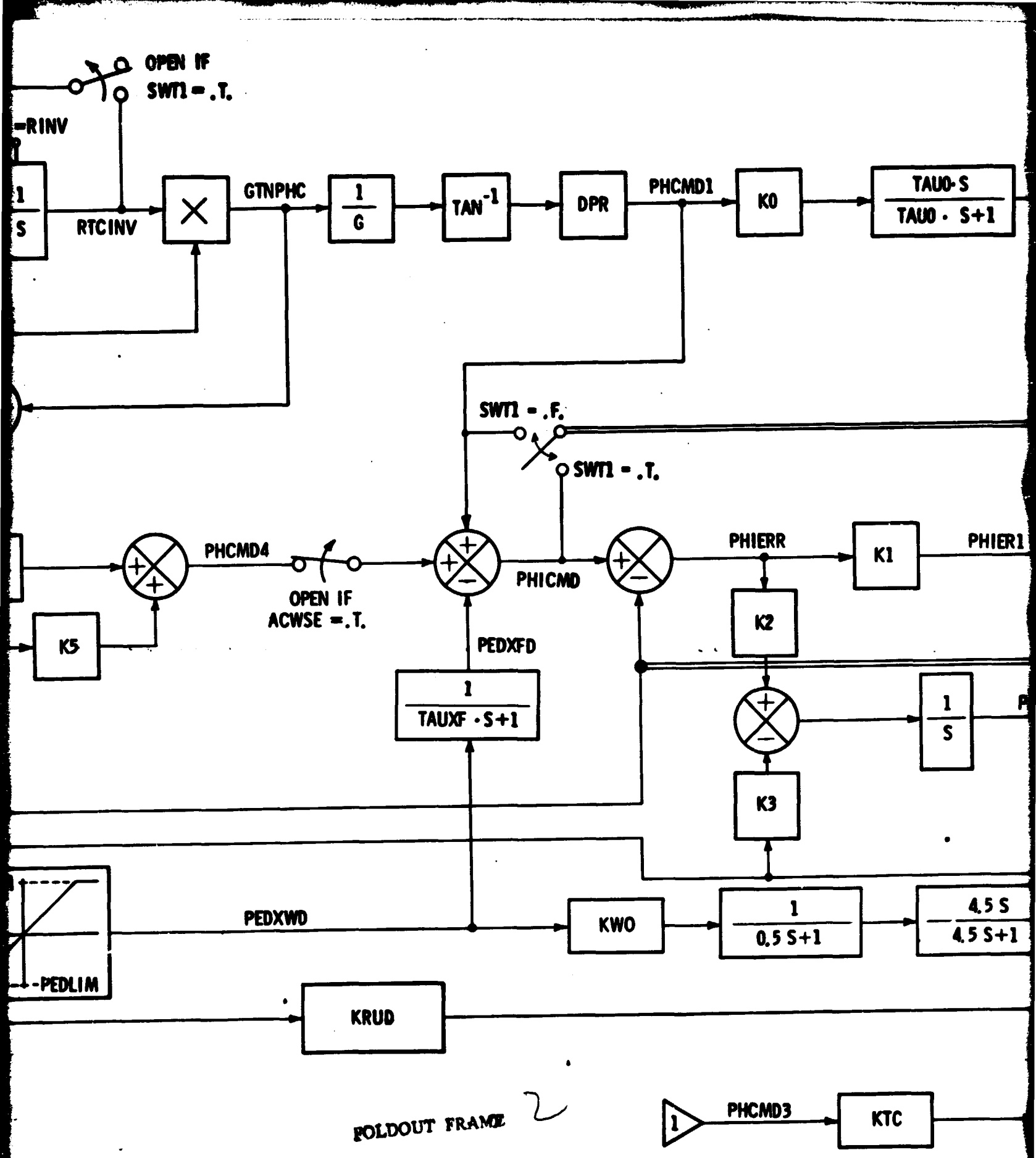

FIGURE 18. LATERAL VELOCITY CWS CONTROL LAW

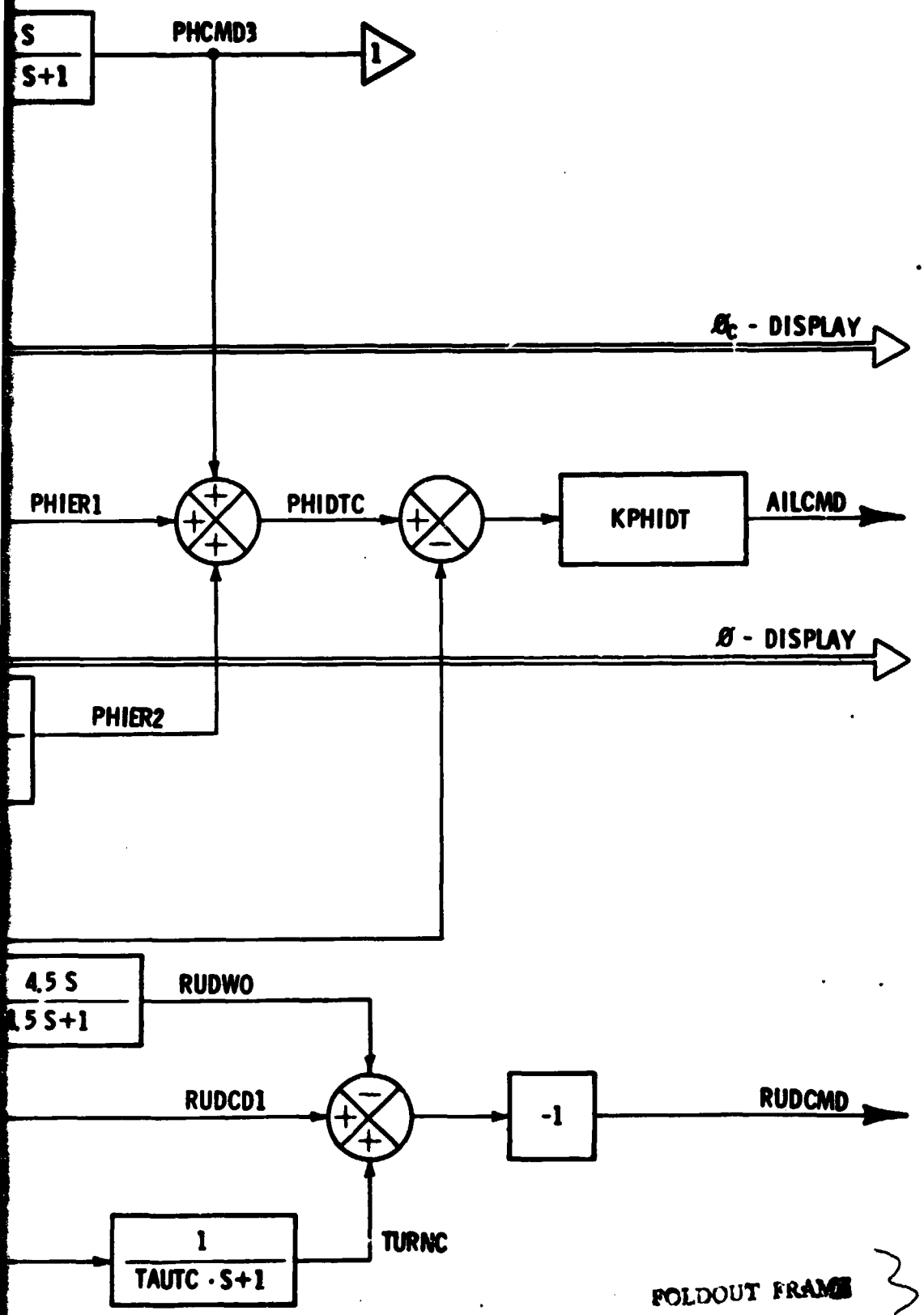

OL LAW CONFIGURATION D.

NOTES

A. ALL INTEGRATORS AND F
RINV = G •

B. SEE FIGURE 10 FOR THI

C. SEE FIGURES 11 AND 12

D. DCRBSW = (FLAPS .GT. 2

E. CONSTANTS: G = 32.17

F.

WHERE TAUX1 = 1.33 AN

G. KTC IS A FUNCTION OF

H. NOMINAL GAINS, TIME

KDW	= 0.2808
KP	= 5.0
TAUD	= 0.5
K0	= 1.4
K1	= 0.5
K2	= 0.7
K3	= 0.5
K4	= 0.5

I. $K6 = \begin{cases} 1. & , IC \\ 0. & , IC \end{cases}$

J. IC2 = RCWOD .OR. (

NOTES

A. ALL INTEGRATORS AND FILTERS ARE INITIALIZED TO ZERO EXCEPT AS INDICATED.
RINV = G * TAN(PHI / DPR) / VGS**2

B. SEE FIGURE 10 FOR THE LOGICAL VARIABLES RCWOD, SWT1, AND IC1.

C. SEE FIGURES 11 AND 12 FOR THE RELATIVE TRACK ANGLE COMMAND SIGNAL XTKX.

D. DCRBSW = (FLAPS .GT. 25.) .AND. VCWSE

E. CONSTANTS: G = 32.17 FT/SEC^2 AND DPR = 57.30 DEGREES/RADIAN.

F. $$TAUX = \begin{cases} TAUX1, & RCWOD = .T. \\ TAUX2, & RCWOD = .F. \end{cases}$$

WHERE TAUX1 = 1.33 AND TAUX2 IS CALCULATED ACCORDING TO THE FOLLOWING SCHEDULE:

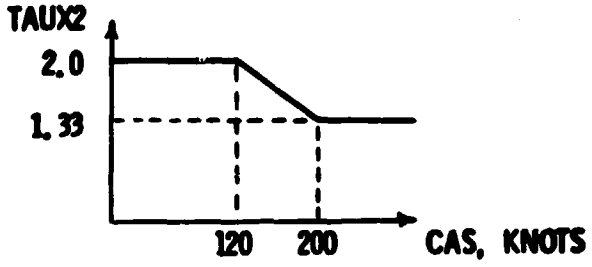

G. KTC IS A FUNCTION OF FLAPS AS SHOWN:

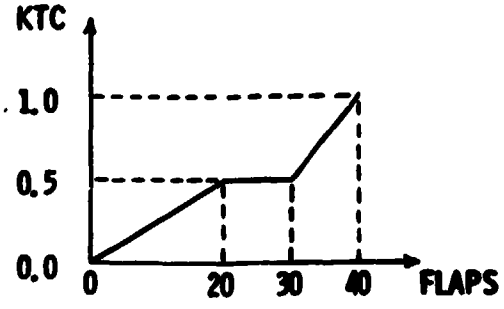

H. NOMINAL GAINS, TIME CONSTANTS, AND LIMITS:

KDW	= 0.2808	K5	= 0.05	TAUTC	= 2.5
KP	= 5.0	K7	= 0.6	WHLIM	= 20.0
TAU0	= 0.5	KPHIDT	= 5.0	PEDLIM	= 5.0
K0	= 1.4	KDELR	= 2.5	ROLIM	= 2.5 } SEE FIGURE 10.
K1	= 0.5	TAUXF	= 1.0	PHILIM	= 1.0 }
K2	= 0.7	KWO	= 0.5	DEGINC	= 0.5 } SEE FIGURE 12.
K3	= 0.5	KRUD	= 6.55	RADINC	= 8.7266 x 10^{-3} }
K4	= 0.5				

I. $$K6 = \begin{cases} 1., & IC1 = .T. \\ 0., & IC1 = .F. \end{cases}$$

J. IC2 = RCWOD .OR. (.NOT. SWT1 .AND. IC1)

FOLDOUT FRAME 4

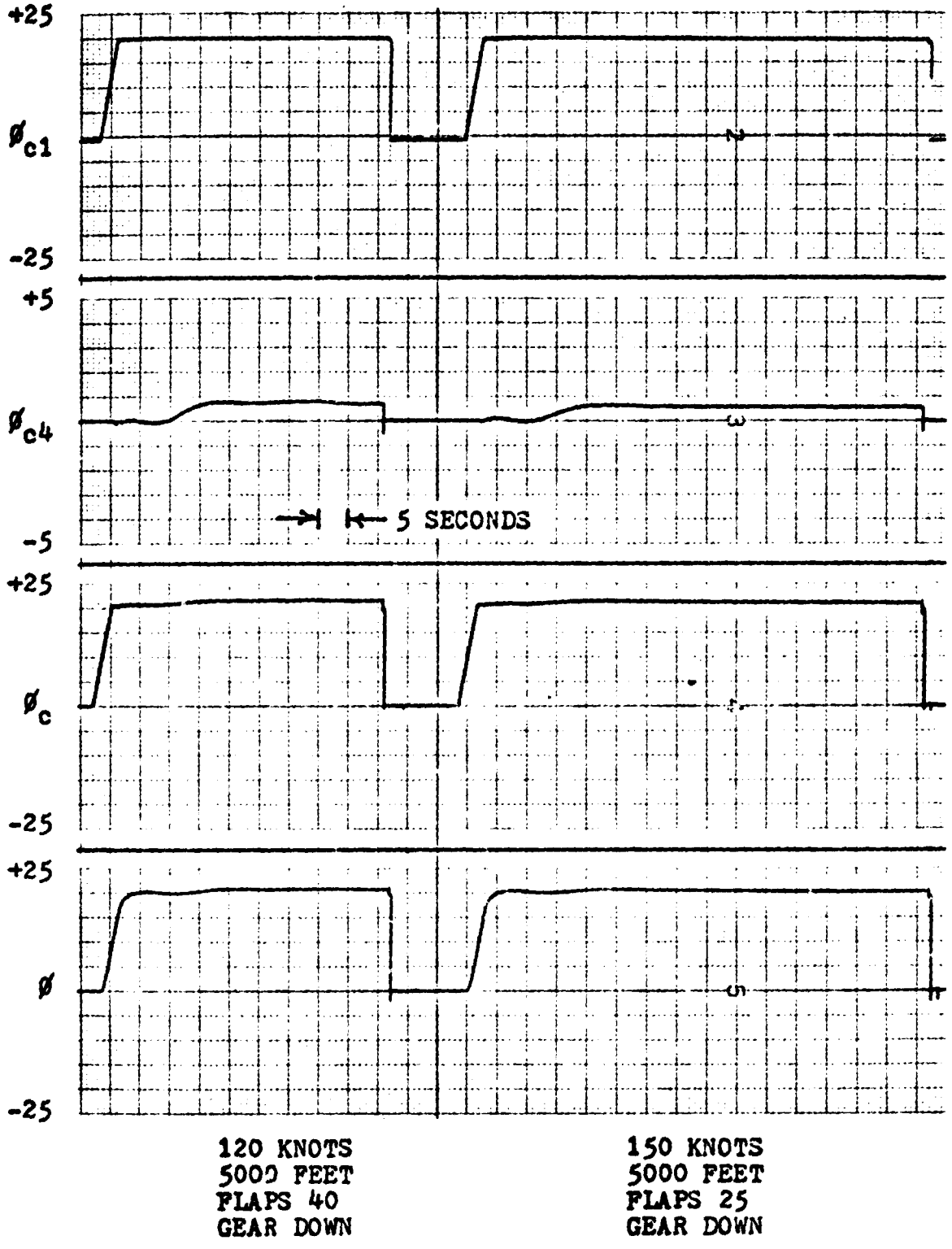

Figure 19. Configuration D roll response from RTS.

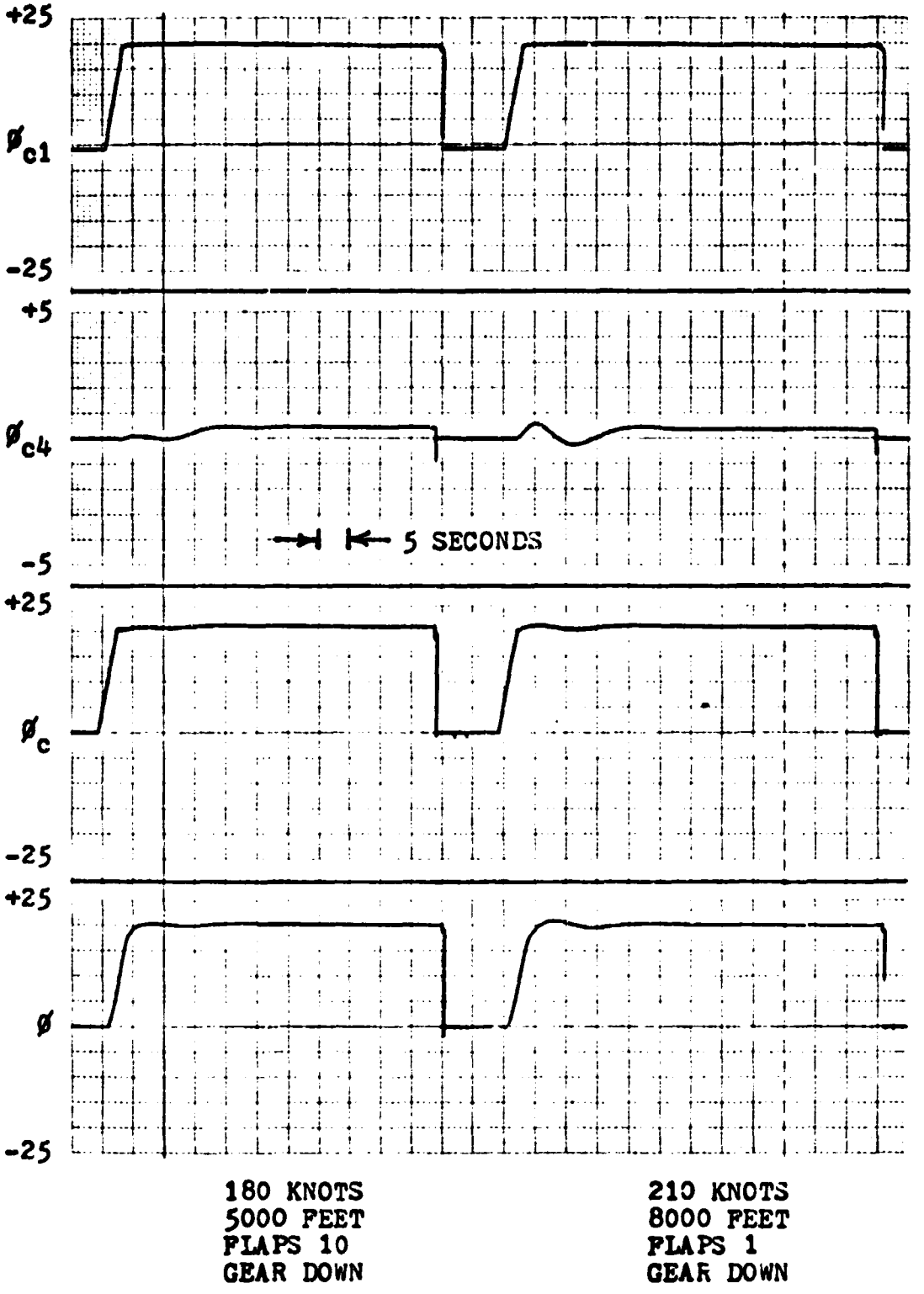

Figure 19. (continued)

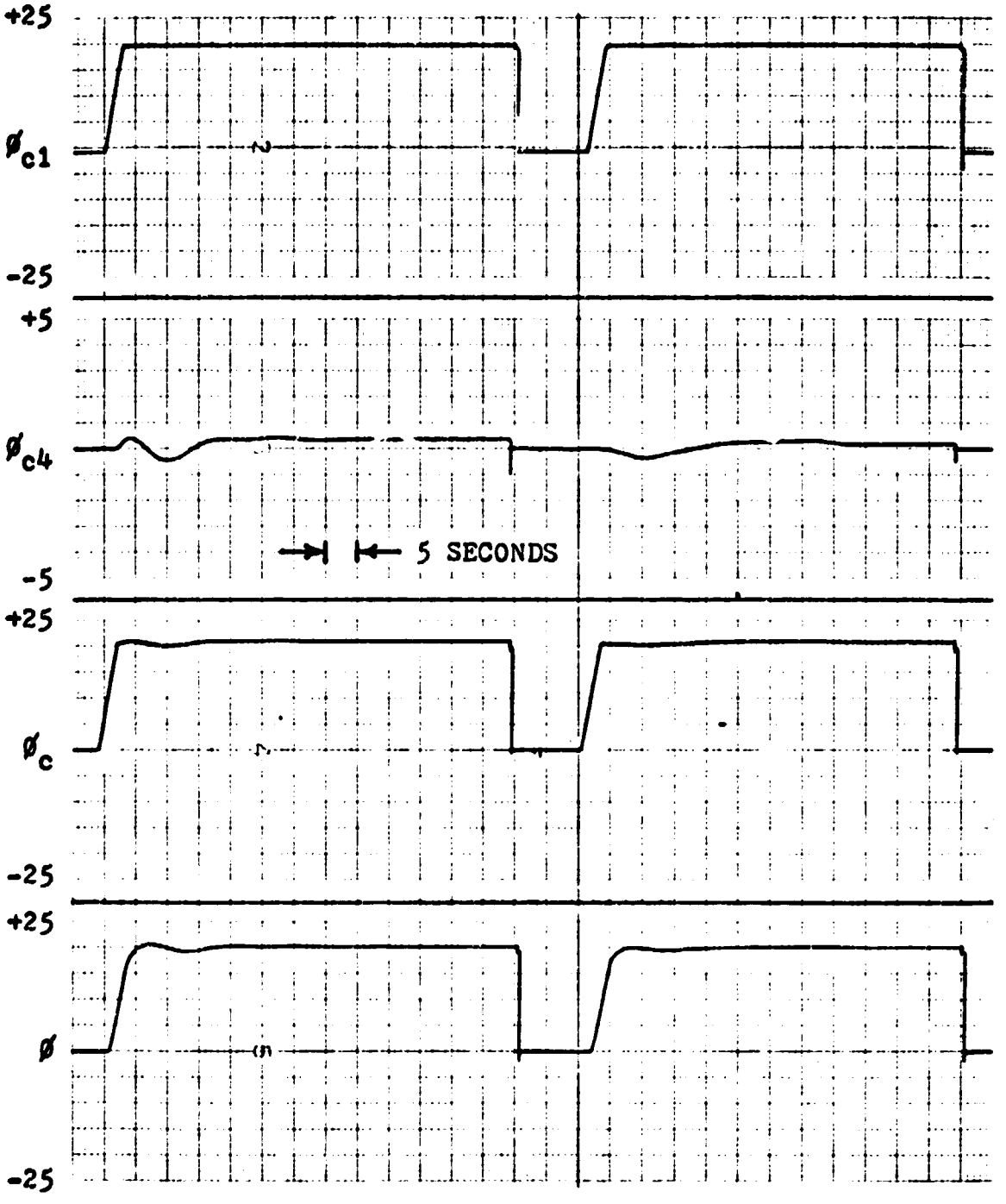

Figure 19. (continued)

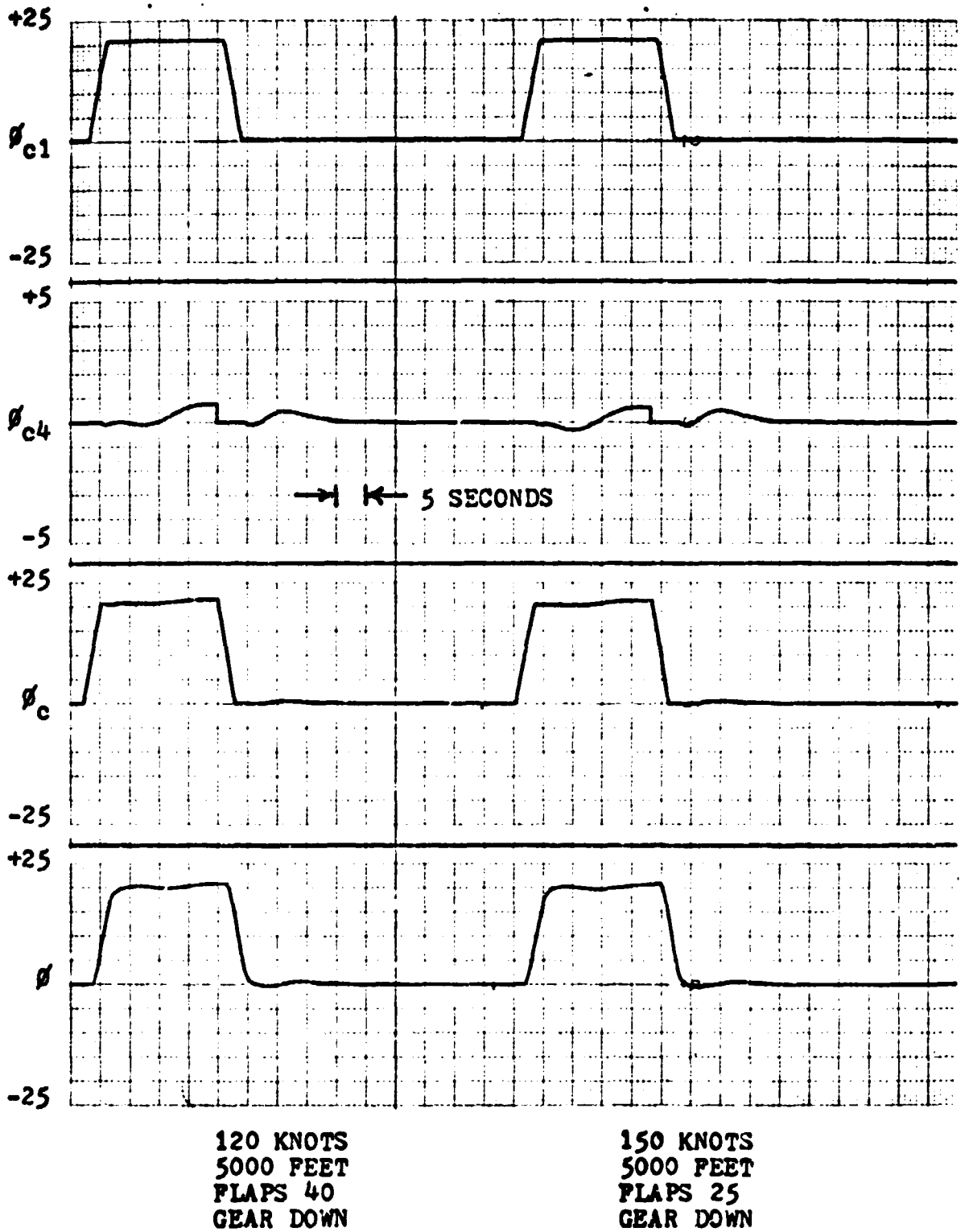

Figure 20. Configuration D wings-level track-hold response from RTS.

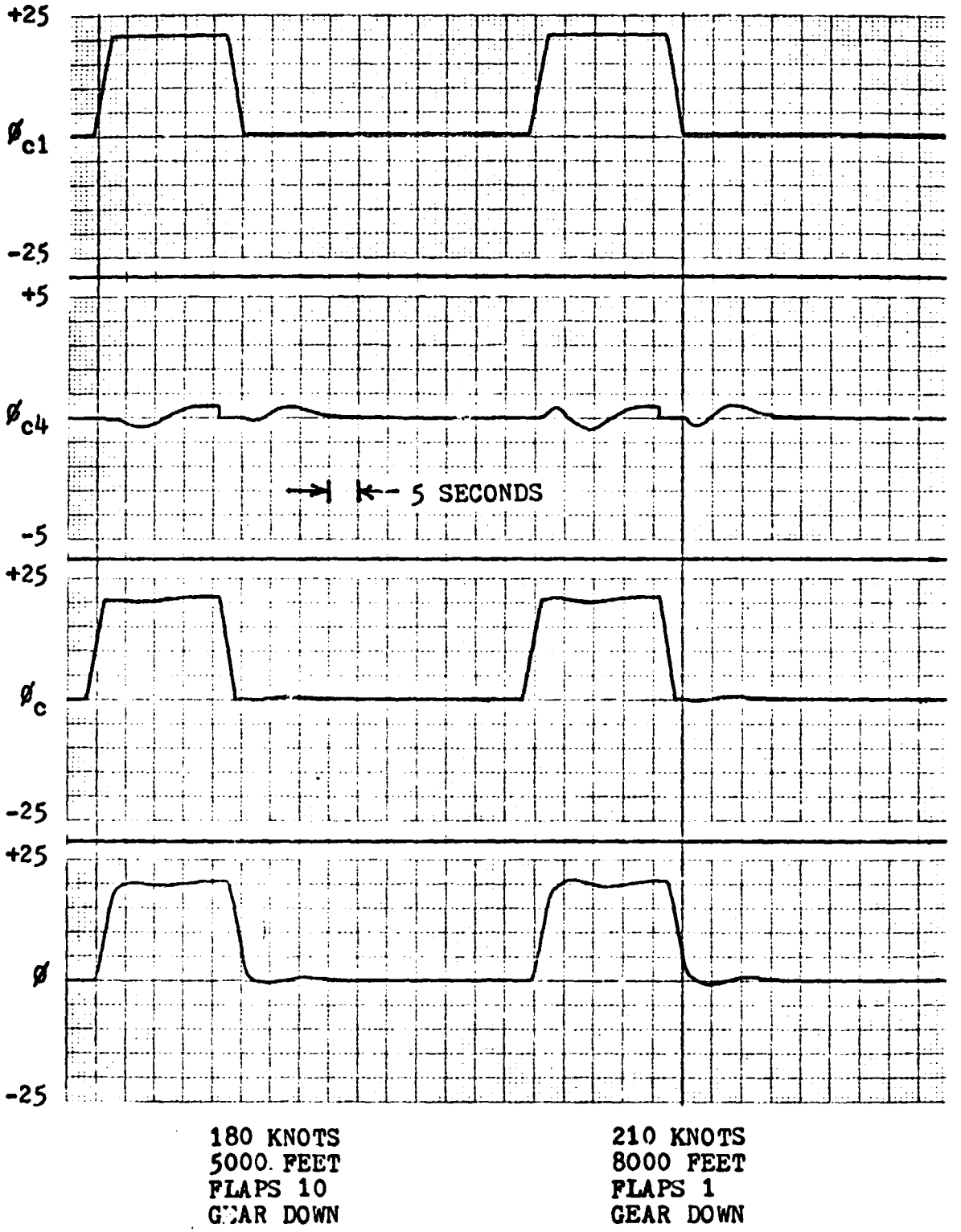

Figure 20. (continued)

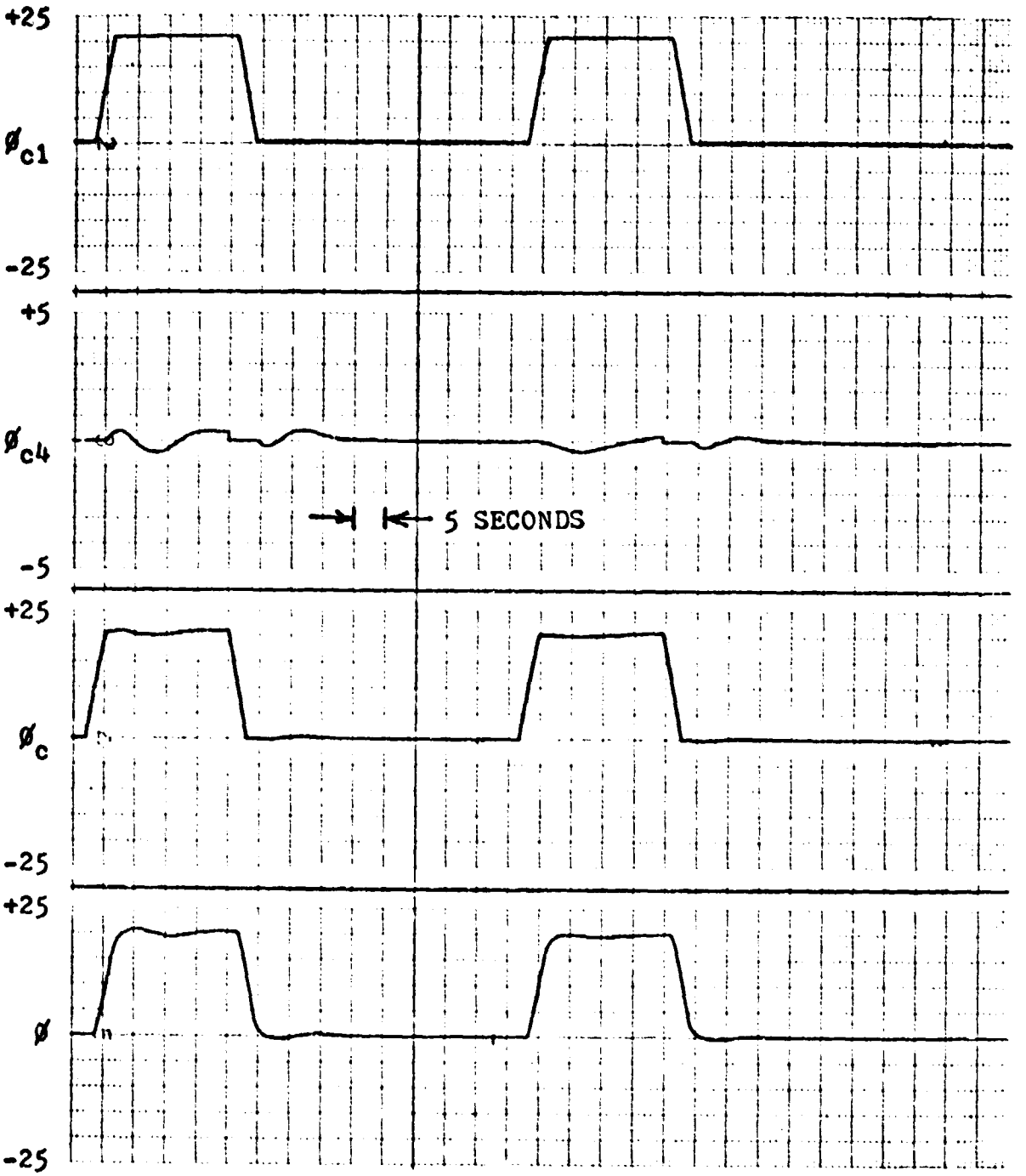

Figure 20. (continued)

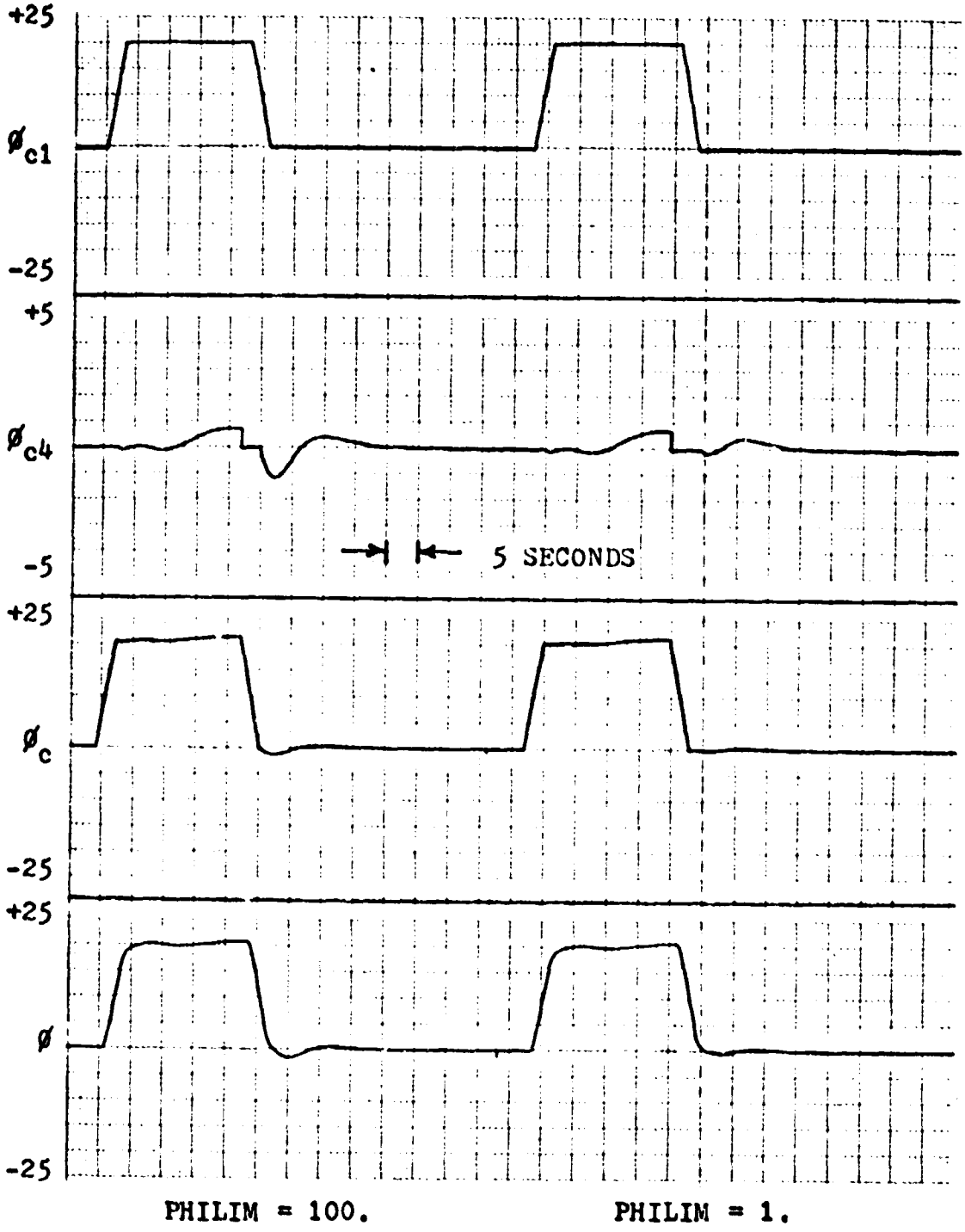

Figure 21. Effect of PHILIM on wings-level track-hold response.

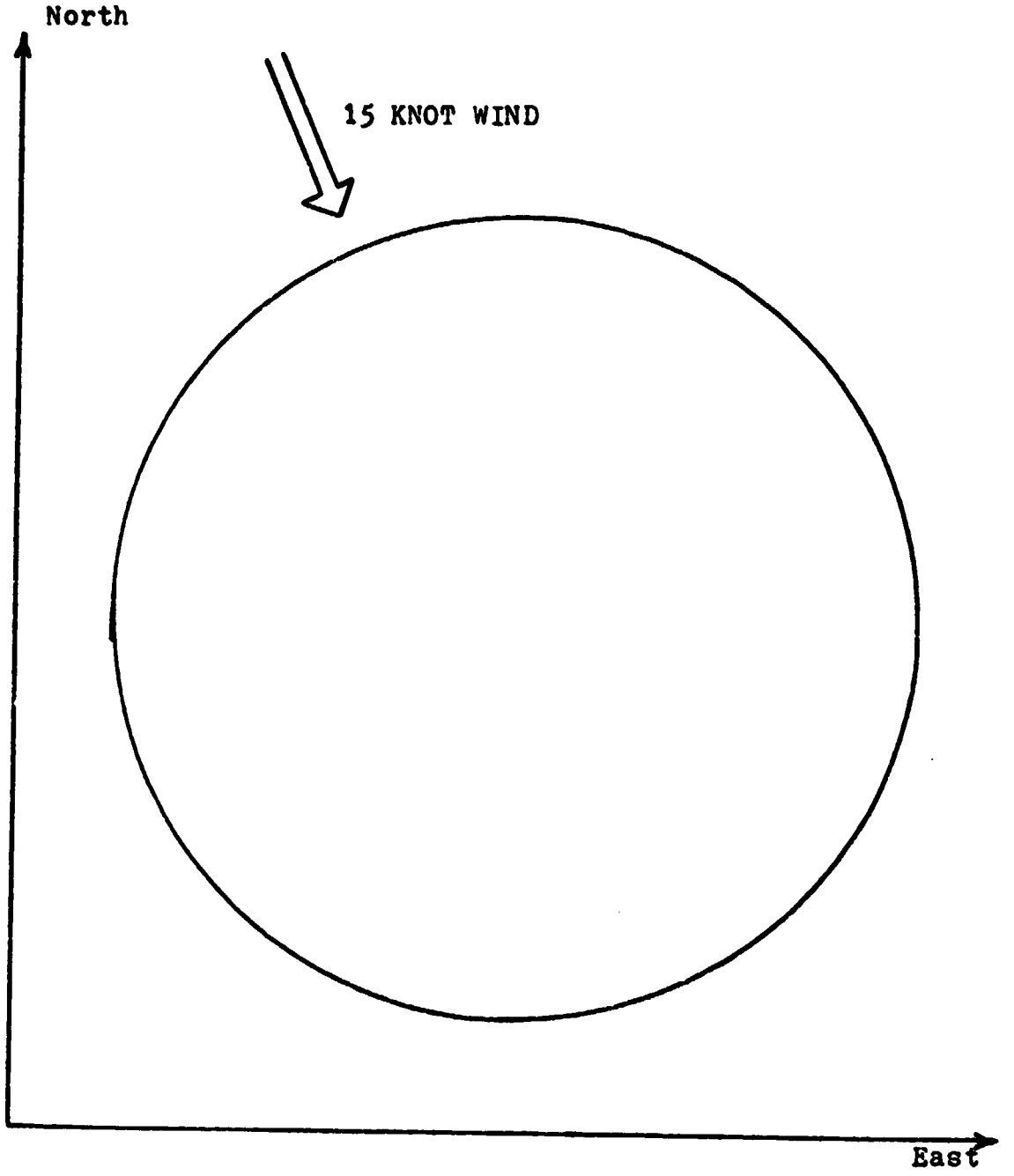

Figure 22. Configuration D ground track in a steady wind.

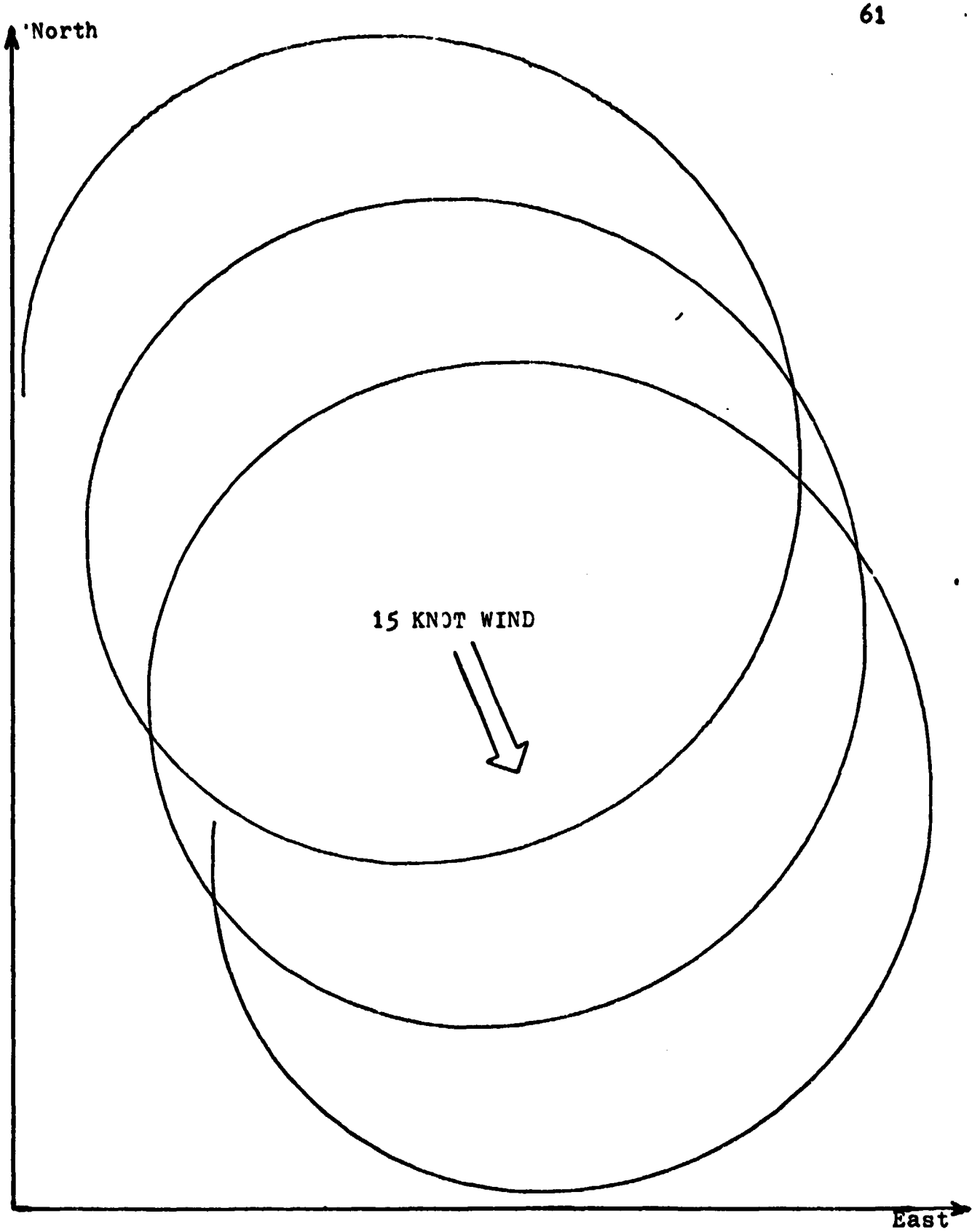

Figure 23. Configuration C ground track in a steady wind.

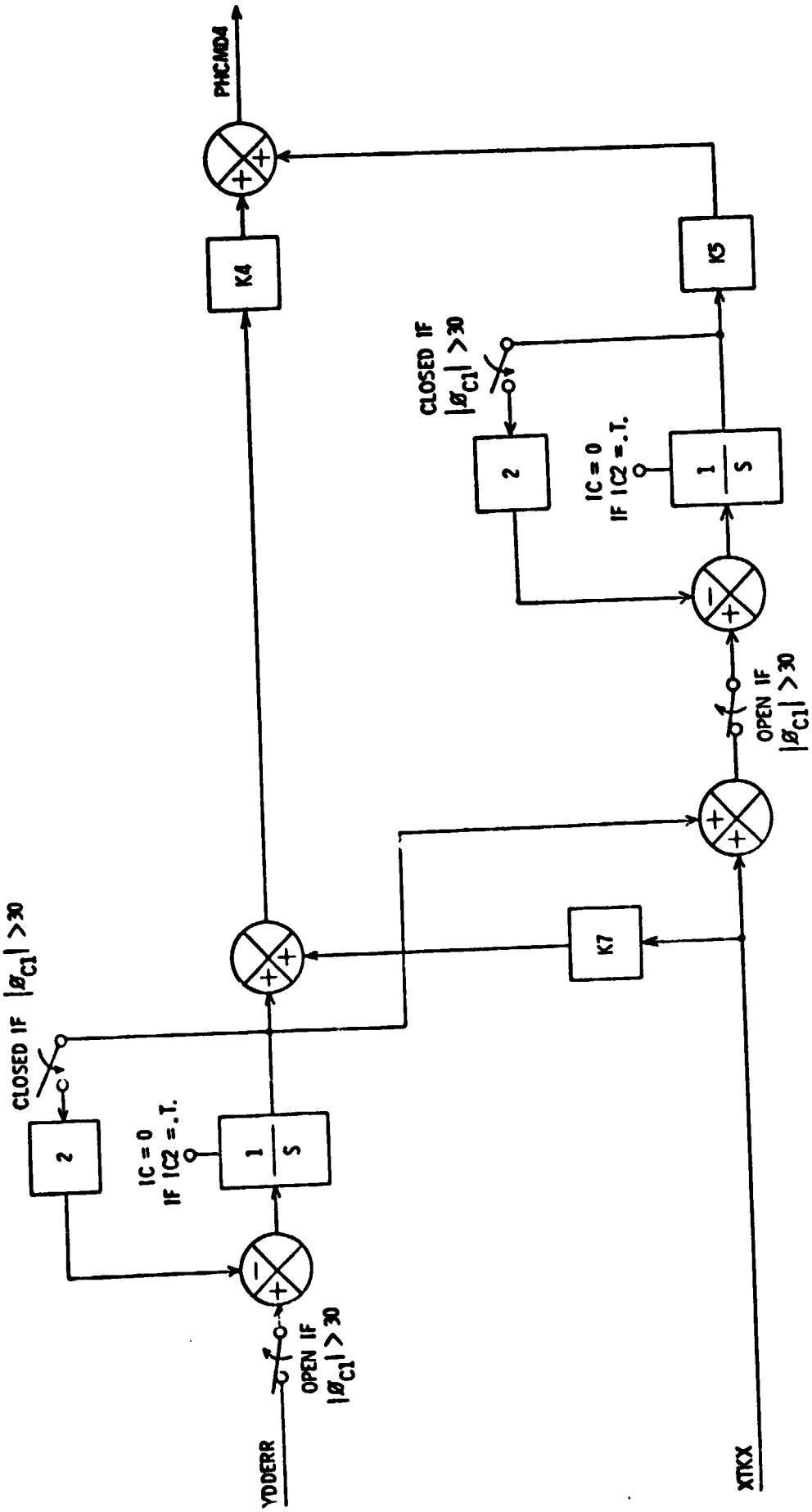

Figure 24. Modified XTK-loop for configuration D.

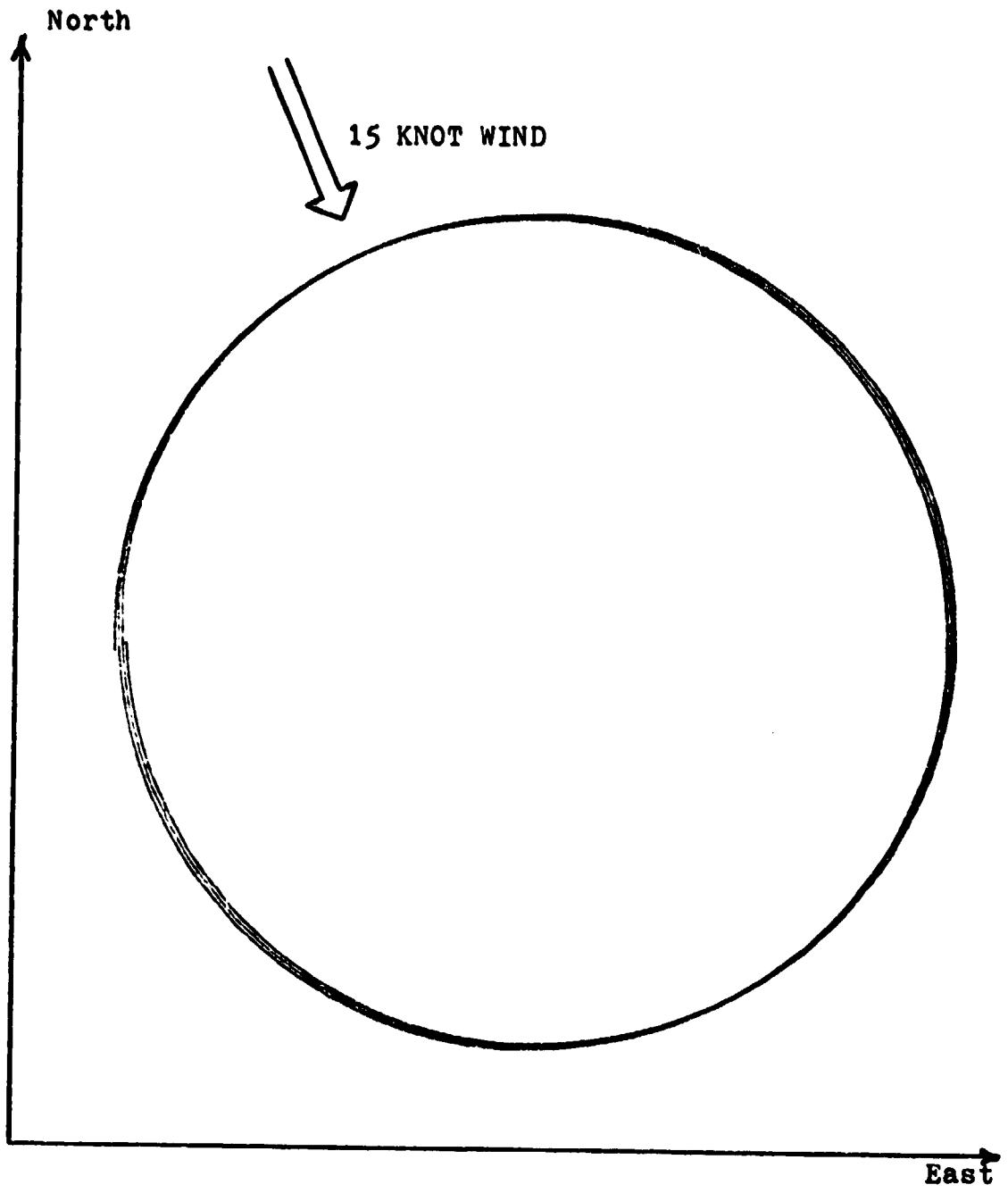

Figure 25. Configuration D curved-track-hold performance without XTK-loop.

REFERENCES

[1] J. P. Reeder, R. T. Taylor, and T. M. Walsh, "New Design and Operating Techniques for Improved Terminal Area Compatibility," Society of Automotive Engineers Air Transportation Meeting, Dallas, Texas, April 30 - May 2, 1974.

[2] A. A. Lambregts and D. G. Cannon, "Development of a Control Wheel Steering Mode and Suitable Displays that Reduce Pilot Workload and Improve Efficiency and Safety of Operation in the Terminal Area and in Windshear," AIAA Guidance and Control Conference, Boulder, Colorado, August 6 - 8, 1979.

[3] A. A. Lambregts, "Development of a Pitch Velocity Control Wheel Steering Control Law and Display System," The Boeing Company, Document No. D6-32868, December 6, 1978.

[4] Memorandum SYST-B8718-N79-126, "TR A-101: Recommendations for an Improved Lateral Control Wheel Steering Implementation," D. G. Cannon to J. F. Creedon et. al., July 11, 1979.

[5] R. Hansen, NASA 515 Roll Attitude Loop Stability Investigation," The Boeing Company, Document No. D6-42695 TN, December 18, 1975.

[6] Broussard and Stallman, "Modification and Verification of an ACSL Simulation of the NASA/Boeing 737 Research Aircraft," Technical Information Memorandum, Information and Control Systems, Inc., August, 1980.